Max-Planck-Institut für Biochemie
Abteilung Strukturforschung

Structural and Biochemical Studies of two Enzymes from the Tetrapyrrole Biosynthetic Pathway: Uroporphyrinogen-III Decarboxylase and Oxygen-dependent Coproporphyrinogen-III Oxidase

Berta Maria Dias Pereira Martins

Vollständiger Abdruck der von der Fakultät für Chemie der Technischen Universität München zur Erlangung des Akademischen Grades eines

Doktors der Naturwissenchaften

genehmigten Dissertation.

Vorsitzender:	Univ.-Prof. Dr. Johannes Buchner
Prüfer der Dissertation:	1. apl.-Prof. Dr. Dr. h.c. Robert Huber
	2. Priv.-Doz. Dr. Albrecht Messerschmidt, Universität Konstanz
	3. Univ.-Prof. Dr. Dr. Adalbert Bacher

Die Dissertation wurde am 13.09.2001 bei der Technischen Universität München eingereicht und durch die Fakultät für Chemie am 29.11.2001 angenommen.

Para os meus pais e irmã

Acknowledgements

The present work was carried out in the Abteilung für Strukturforschung at the Max-Planck-Institut für Biochemie, Martinsried, Germany under the supervision of Prof. Dr. Robert Huber, FRS. The successfully accomplishment of this Thesis was only possible with the (in)direct participation from several financial institutions, and exceptional people always ready to give a hand or a shoulder according to the situation.

Let me start with the financial support. First, my parents who not vacillating when confronted with my decision of leaving the *sunny, easy-living* Portugal to come to the *cold, dark and fish-lacking* Bavaria immediately came up with a *small emergency check* for the first days. Secondly, Prof. Dr. Robert Huber who promptly accepted to support me during the initial struggles to obtain the Ph.D. fellowship. I'm also grateful to the Fundação para a Ciência e a Tecnologia, Ministério da Ciência, Portugal, which through the Programa PRAXIS XXI allows Portuguese students to start their scientific carrier abroad. Last but not lest, I would like to thank all entities that turn possible my attendance at workshops and conferences.

Turning now to the people who helped me to successfully accomplish this Thesis. I would like to start by thanking Prof. Dr. Robert Huber for his continuous support over the past years and his incentive to independently research on projects of my interest. A grateful thanks goes to PD Dr. habil. Albrecht Messerschmidt for his interest in my work, support and friendly advice. I'm also grateful to Prof. Dr. Bernhard Grimm (Humbolt Universität zu Berlin, Germany) and Dr. Hans-Peter Mock (IPK, Gatersleben, Germany) for the very nice collaboration on tobacco UROD. A very special thanks to Sofia "Maria Flor" Macieira for the unforgettable great times while working on the bacterial Oxygen-dependent CPO. I would like to acknowledge Dr. Gerald Richter (TUM), Frau Lissy Weyher-Stingl, and Frau Sylvia Koerner and Dr. Frank Siedler for their valuable help during the ultracentrifugation, CD spectroscopy and ES mass spectometry, respectively.

I would like to thank Dr. Sandra de Macedo-Ribeiro (now at the University of Faro, Portugal) for her friendship and for introducing me to the world of crystallography. Sandra, together with Dr. Tewfik Soulimane (PSI, Swiss) lent me a precious hand upon the impossibility to go further with my original Thesis' project by sharing with me one of her projects (structural determination and analysis of a thermostable electron carrier protein). To

Dr. Uwe Jacob I want to thank his generous help in the beginning of the UROD project and helpful discussions thereafter. I would like to acknowledge Prof. Dr. José Moura (FCT, UNL, Portugal) for his incentive during the university studies and friendly support thereafter, and Prof. Dr. M. João Romão (FCT, UNL, Portugal) for letting me participate in the initial steps of several interesting projects. I'm grateful to Prof. Dr. Claudina Rodrigues-Pousada and Orfeu Flores (ITQB, Portugal), who patiently guided my first steps in science for their friendly encouragement.

To all my friends and colleagues still struggling around or somewhere else a big kiss of thanks, two for the *Iberian Connection*. The jovial atmosphere in our department is the result from combining freedom of research, a bunch of colleagues and friends and the excellent work from a hand full of people, who make us believe in miracles with their willingness to help overcome the most various obstacles. My most sincere acknowledgements to Frau Renate Rüller, Frau Gina Beckmann, Frau Langer (travel's office), Herr Snézan Marinkovic, Herr Werner Dersch and Herr Ottmar Paul.

My stay in Martinsried brought me lots of happy occasions but also moments of deep frustration. Holger's smile helped me using the happiness to diminish the deceptions. His constant support, *Prussian* patience and cheerful humour have been a balsam to my Mediterranean *hectic* soul. Closing the cycle, I want to express my gratitude to my parents and sister for their unbreakable love, patience and confidence.

Table of Contents

1 Summary

The tetrapyrrole ring system has been adopted by living systems as a chelating agent for the metal ions Mg^{+2}, Fe^{+2}, Co^{+2} and Ni^{+2}. The resulting prosthetic groups and cofactors (bacterio)-chlorophyll, heme, siroheme, vitamin B_{12} and cofactor F_{430}, produced by the diverse branches of the tetrapyrrole biosynthetic pathway cover a wide spectrum of versatility and are employed for many vital roles in bioenergetics.

The complex enzymatic catalysis involved in the forked tetrapyrrole biosynthesis is slowly becoming unravelled. During the last decades, work done on the biochemical and structural fields has contribute to the current knowledge about its several branching pathways. To gain further insight into the complex enzymatic catalysis involved in this metabolism, two enzymes were studied in the present work, namely uroporphyrinogen-III decarboxylase and coproporphyrinogen-III oxidase. Uroporphyrinogen-III decarboxylase catalyses a four-step decarboxylation converting the universal tetrapyrrolic precursor uroporphyrinogen-III into coproporphyrinogen-III, which is then converted into protoporphyrinogen-IX through a two-step oxidative decarboxylation catalysed by coproporphyrinogen-III oxidase.

• **Uroporphyrinogen-III Decarboxylase** from the plant *Nicotiana tabacum* (tobacco) (6.1) was biochemical and structurally characterised in an attempt to explain its unique catalysis, and to further understand its physiologic relevance for heme and chlorophyll biogenesis, photosynthesis and antioxidative stress defence. Due to the lack of structural information on the substrate enzyme interaction, the substrate enzyme complexes for tobacco and human enzymes were modelled.

The structural comparison of the tobacco enzyme with its homologous human protein reveals a similar catalytic cleft with six invariant polar residues. Additionally, the functional relationships obtained from the structural and modelling analyses allowed the proposal for a refined catalytic mechanism. Asp82 and Tyr159 seem to be the catalytic functional groups while the other residues may serve in substrate recognition and binding, with Arg32 steering its insertion into the *less attractive* hydrophobic catalytic cleft.

The observed crystallographic dimer appears to represent the protein dimer under physiological conditions. The degree of amino acid conservation involved in the dimer interface, together with an almost identical interface observed in the homologous human

protein suggests that the dimer is a general property in this enzyme family. Furthermore, the dimeric arrangement offers a plausible mechanism at least for the first two (out of four) decarboxylation steps.

- **Oxygen-dependent Coproporphyrinogen-III Oxidase** from *E. coli* (6.2) was over-expressed and purified to homogeneity in one-step purification at a level of roughly 20 mg per culture litre. This high yield purification allowed the biochemical characterisation and the initialisation of structural studies.

The protein dimer displays a compact shape, most probably due to its hydrophobic character. Since all its characterised counterparts adopt a dimeric form in solution, the dimer may be a common property to all members of this enzyme family. The presence of substrate or product tightly associated with the dimeric form suggests a physiological relevance for the dimer, namely it may be the active unit *in vivo*. Initial crystallisation trials produced crystal plates with an ordered but week diffraction power.

2 Zusammenfassung

Das Tetrapyrrol-Ringsystem wird als Komplexligand für die Metallionen Mg^{2+}, Fe^{2+}, Co^{2+} and Ni^{2+} in lebendigen Systemen verwendet. Die dadurch gebildeten prosthetischen Gruppen und Kofaktoren, (Bakterio)-Chlorophyll, Häm, Sirohäm, Vitamin-B_{12} und Kofaktor F_{430}, sind die Endprodukte der verzweigten Tetrapyrrolbiosynthese und spielen in vielen bioenergetischen Prozessen eine zentrale Rolle.

Strukturelle und biochemische Arbeiten der letzten Jahrzehnte erlaubten zwar die Identifizierung der meisten Enzyme der Tetrapyrrolbiosynthesen, doch ist die mechanistische Seite dieser Prozesse noch wenig verstanden. Ein Beitrag zur Klärung dieser offenen Fragen wurde im Rahmen dieser Arbeit versucht, in der zwei Enzyme, die Uroporphyrinogen-III Decarboxylase und die sauerstoff-abhängige Coproporphyrinogen-III Oxidase, strukturell und biochemisch untersucht wurden.

Uroporphyrinogen-III Decarboxylase katalysiert eine Decarboxylierung in vier Schritten und wandelt dabei den universellen Tetrapyrrolvorläufer Uroporphyrinogen-III zu Coproporphyrinogen-III um, welcher dann in einer oxidativen Decarboxylierung in zwei Schritten durch die Coproporphyrinogen-III Oxidase weiter umgesetzt wird zu Protoporphyrinogen-IX.

- **Uroporphyrinogen-III Decarboxylase** aus *Nicotiana tabacum* (Tabakpflanze) (6.1) wurde zur Klärung ihrer einzigartigen Katalyse und ihrer physiologischen Bedeutung für die Häm- und Chlorophyllbiosynthese biochemisch und strukturell untersucht. Da kristallographische Informationen über die Substratbindung bislang fehlen, wurden Enzym-Substrat Komplexe für die humane und pflanzliche Enzymstruktur *in-silico* modelliert.

Der Strukturvergleich des pflanzlichen Enzyms mit dem homologen humanen Protein zeigt ähnliche katalytische *clefts*, die von sechs invarianten polaren Reste flankiert werden. Die strukturelle Analyse zusammen mit Modellierungsstudien erlaubten eine weitere Differenzierung des katalytischen Mechanismus. Dabei konnten Asp82 und Tyr159 als die katalytische wichtigen Reste identifiziert werden, während die anderen Reste an der Substraterkennung und -bindung teilnehmen. Arg32 wirkt dabei wie ein polarer Ladearm, der das Substrat in die abweisende hydrophobe Umgebung der katalytischen *cleft* bringt.

Die Packungsanalyse der pflanzlichen wie der humanen Kristallstruktur legt das Vorhandensein von Dimeren nahe, welche auch unter physiologischen Bedingungen existieren. Die ausgeprägte Konservierung von Resten im Dimerinterface, zusammen mit dem praktisch identischen Interface in der humanen Struktur lassen den dimeren Aufbau als eine generelle Eigenschaft innerhalb dieser Enzymfamilie vermuten. Zusätzlich erlaubt die dimere Anordnung einen plausible Erklärung für die ersten zwei Decarboxylierungsschritte.

- **Sauerstoff-abhängige Coproporphyrinogen-III Oxidase** aus *E. coli* (6.2) konnte nach rekombinanter Überexpression in einem Affinitätsreinigungsschritt mit einer Ausbeute von bis zu 20 mg pro Liter Kulturmedium isoliert werden. Die hohe Ausbeute erlaubte die biochemische Charakterisierung und erste Schritt auf dem Weg zur einer Kristallstruktur.

Das Proteindimer zeigt eine kompakte Form, die wahrscheinlich im hydrophoben Charakter des Proteins begründet liegt. Nachdem alle charakterisierten Mitglieder dieser Enzymfamilie in Lösung als Dimere auftreten, erscheint dies eine allgemeine Eigenschaft der Coproporphyrinogen-III Oxidasen zu sein. Gebundenes Substrat oder Produkt, das mit der dimeren Form zusammen auftritt, läßt eine physiologishe Bedeutung des Dimers als aktive Form *in vivo* wahrscheinlich erscheinen. Erste Kristallisationsversuche ergaben geordnete Kristallplättchen, mit geringer Beugungskraft.

3 Sumário

O anel tetrapirrólico é usado pelos sistemas biológicos como agente quelante dos iões metálicos Mg^{2+}, Fe^{2+}, Co^{2+} and Ni^{2+}. Os grupos prostéticos e cofactores dele resultantes, tais como a (bacterio)-clorofila, o hemo, o sirohemo, a vitamina B_{12} e o cofactor F_{430}, produtos finais dos vários ramos da via metabólica para a síntese de compostos tetrapirrólicos, são utilisados em muitos dos processos bioenergéticos vitais.

A complexidade da catálise enzimática presente na biosíntese de compostos tetrapirrólicos tem vindo a ser revelada gradualmente. O conhecimento actual sobre os seus diversos ramos metabólicos, tem evoluído nas últimas decadas, devido especialmente à contribuição de diversos estudos bioquímicos e estruturais. De forma a melhor compreender a complexa actividade enzimática envolvida neste metabolismo, no presente trabalho foram estudadas duas enzimas: descarboxilase do *uroporfirinogénio*-III e oxidase do *coproporfirinogénio*-III. A primeira cataliza uma descarboxilação em quatro passos convertendo o *uroporfirinogénio*-III (precursor universal de compostos tetrapirrólicos) em *coproporfirinogénio*-III, que é de seguida convertido em *protoporfirinogénio*-IX através de uma descarboxilação oxidativa catalizada pela segunda enzima.

- A enzima **Descarboxilase de *uroporfirinogénio*-III** da planta *Nicotiana tabacum* (tabaco) (6.1) foi caracterizada bioquímica e estruturalmente com o intuito de explicar a sua peculiar catálise enzimática, e para melhor compreender a sua importância fisiológica na biosíntese do hemo e clorofila, na fotossíntese e na defesa antioxidativa. Foram criados modelos dos complexos enzima-substrato, para as enzimas humana e do tabaco, de forma a tentar suprir a falta de dados experimentais sobre o modo de interaccção entre a enzima e o substrato.

A comparação estrutural entre as duas enzimas mostrou a similariedade entre os respectivos centros catalíticos com seis resíduos polares invariante. A análise das estruturas cristalográficas e dos complexos modelados permitiu aumentar de forma substancial a informa invariante disponível sobre o meanismo enzimático. Os aminoácidos Aspartato 82 e Tirosina 159 constituem os grupos catalíticos mais prováveis, enquanto que os restantes resíduos poderão estar involvidos no reconhecimento e ligação do substrato. A Arginina 32

funcionaria como grupo polar chave para a inserção do substrato no centro catalítico essencialmente hidrófobo.

O dímero formado pela proteína *in vivo* parece estar reproduzido no cristal através do dímero cristalográfico. O grau de conservação da estrutura primária envolvida na interface dimérica, em conjunto com a semelhança com o dímero formado pela proteína humana homóloga, é uma forte indicação de que a dimerização constitui uma propriedade geral desta classe enzimática. Além disso, o arranjo dimérico oferece um mecanismo plausível para pelo menos os dois primeiros passos (de um total de quatro) da descarboxilação enzimática.

• A enzima **Oxidase de *coproporfirinogénio*-III dependente de Oxigénio** da bactéria *Escherichia coli* (6.2) foi expressa em grandes quantidades e purificada até á homogeneidade, num único passo de purificação com um rendimento de aproximadamente 20 mg de proteína por litro de cultura bacteriana. Este elevado rendimento permitiu a sua caracterização bioquímica e a realização de estudos estruturais.

A proteína forma um dímero em condições fisiológicas. Este dímero apresenta uma forma compacta provavelmente devido ao caractér hidrófobo da proteína. Uma vez que todas as enzimas homólogas já caracterizadas adoptam também um arranjo dimérico em solução, o dímero poderá constituir uma propriedade comum a esta classe enzimática. A presença de substrato ou produto fortemente associado à forma dimérica sugere uma importância fisiológica para o dímero, nomeadamente o de poder ser a unidade activa *in vivo*. Estudos iniciais de cristalização produziram cristais em forma de placas que mostraram um fraco, mas ordenado padrão de difracção de raios-X. Estes estudos constituem um bom ponto de partida para a futura análise estrutural deste membro representativo da família oxidase de *coproporfirinogénio*-III dependente de oxigénio.

4 Introduction

4.1 Biological Function of Tetrapyrroles

The tetrapyrrole biosynthetic pathway provides crucial prosthetic groups and cofactors that support the enzymatic catalysis of life sustaining processes (Fig. 1). Its significance for living organisms is clearly shown by its widely spread utilisation and high degree of enzymatic conservation, from archaea to mammals (Beale, 1994). Thus the biologically functional metallotetrapyrroles (bacterio)-chlorophyll, heme, vitamin B_{12}, siroheme and factor F_{430}, rank with lipid bilayers, proteins, and the nucleic acids as critical components of living systems.

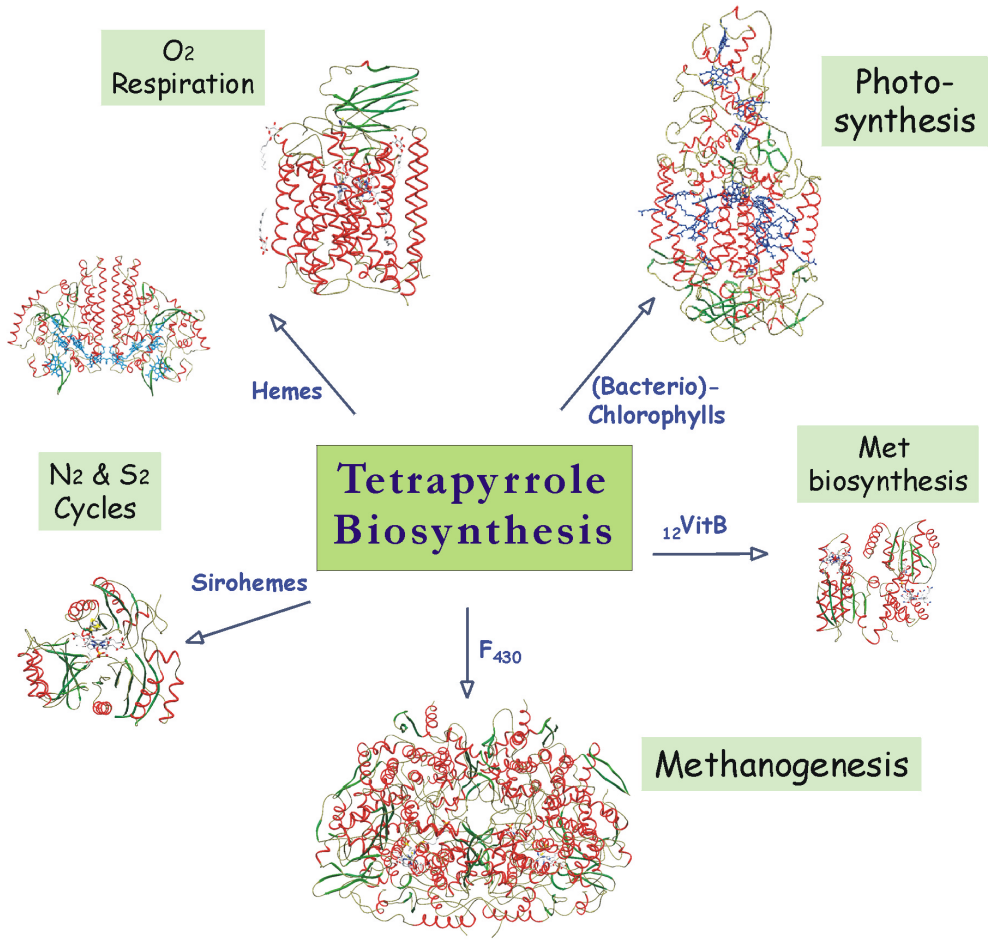

Figure 1 - Biological relevance of the tetrapyrrole metabolism. Examples of the essential biological processes of life, together with some of their supporting enzymes are displayed.

While no species is capable of forming all of those tetrapyrroles end products, a single organism often forms varying amounts of two or more simultaneously or at different stages of development. For instance, chlorophyll, heme and siroheme are synthesised in plants, and *E. coli* has the capability to produce heme, vitamin B_{12} and siroheme. This complex biosynthetic pathway requires a high degree of metabolic control. Negative feedback, for example by heme, is often found (Woods, 1974). Additionally, the correct assembly of the tetrapyrrole molecules with their respective apoproteins is essential for an efficient cellular function. Thus the need of a tight synchronisation between the tetrapyrrole metabolism and other physiologic processes to ensure an adequate supply of those molecules (Grimm, 1998).

The pathway is broadly similar in all living systems, the first universal tetrapyrrole precursor being δ-aminolevulinic acid (ALA). There are two totally distinct routes by which ALA is produced, one utilising the carbon skeleton of glutamate (C_5 pathway) and the other involving glycine and succinyl-CoA (Succinyl-CoA pathway). Whereas the C_5 pathway is found in plants and most of the biosphere (Beale and Castelfranco, 1973), (Meller *et al.*, 1975), the Succinyl-CoA pathway, although occurring in members of the α proteobacterial group (such as photosynthetic bacteria from the *Rhodobacter* genera and nonphotosynthetic bacteria from the *Rhizobium* genera), is mainly confined to eukaryotic organisms that do not contain chloroplasts (animals and fungi) (Shemin and Russel, 1953). Here, ALA is formed by condensation of glycine with succinyl-CoA in a reaction catalysed by a single enzyme, the pyridoxal-phosphate containing ALA synthase (EC 2.3.1.37) (Gibson *et al.*, 1958) (Kikuchi *et al.*, 1958).

Once formed, ALA is transformed into the first macrocyclic tetrapyrrole precursor, uroprophyrinogen-III (uro-III), in only three enzymatic stages. In the first, two molecules of ALA condense with one another forming the basic pyrrole building block, porphobilinogen (PBG). Next, four molecules of PBG polymerise together in a chain to generate hydroxymethylbilane (HMB). Lastly, HMB is cyclised, with rearrangement of one of the pyrrole rings, the D ring, to yield the key intermediate uro-III.

There are two major forks in the pathway. The first occurs immediately on formation of uro-III. Its decarboxylation and further side chain modifications generates protoporphyrin-IX in route to heme, chlorophyll and bacteriochlorophyll. Alternatively, it may be methylated for transformation into siroheme, vitamin B_{12} or the cofactor F_{430}. The second fork occurs at

the protoporphyrin-IX level branching to the heme and (bacterio)-chlorophyll paths. Figure 2 depicts an overall outline of the tetrapyrrole biosynthetic pathway.

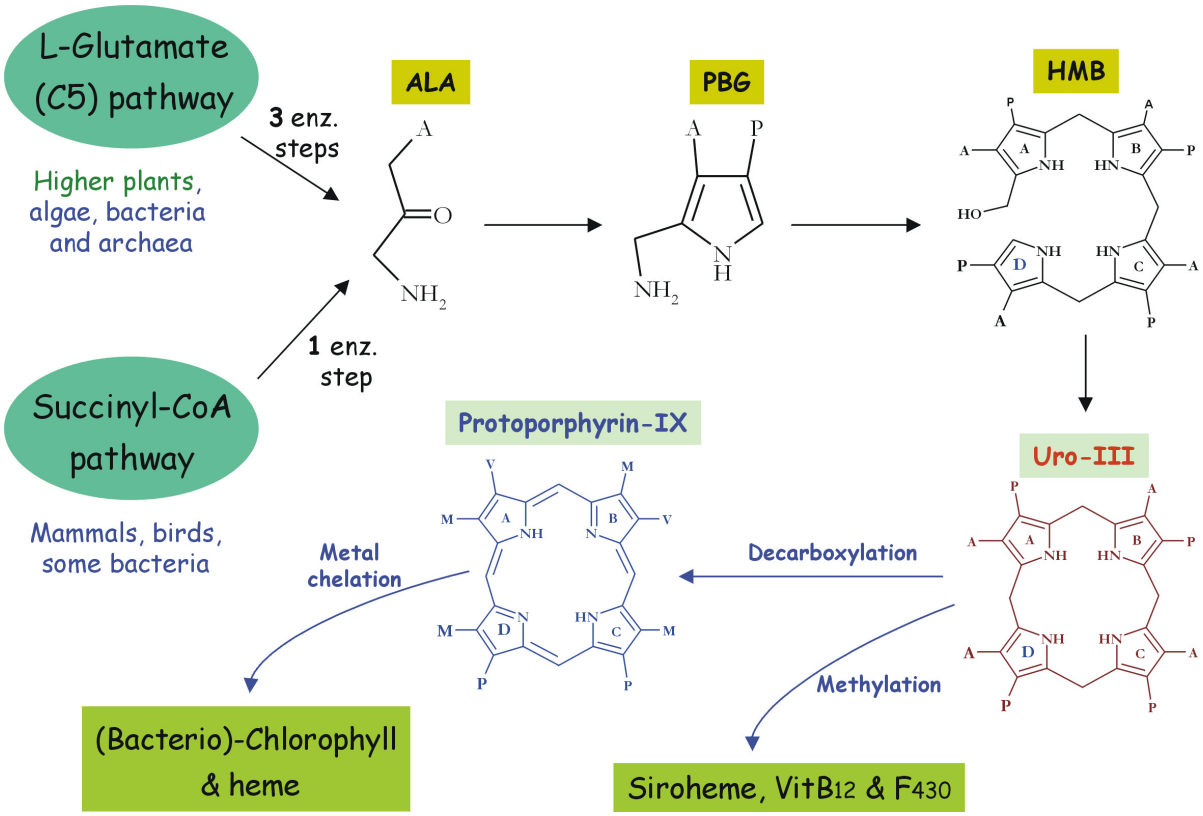

Figure 2 Overall outline of the tetrapyrrole biosynthetic pathway. The intermediates localised at the two main branching points are highlighted in dark red and blue (uro-III and protoporphyrin-IX, respectively).

Whilst the final products from the tetrapyrrole biosynthesis are biologically important, their precursors, when oxidised (porphyrins, Fig. 3B) are not only useless, but also toxic. The physiological intermediates, porphyrinogens (Fig. 3A) *per se* are chemically inert except for a high sensitivity to oxidation. They are colourless, and neither fluoresce nor bind metals ((Wyckoff and Kusnher, 1994), (Kappas *et al.*, 1995) and references within). However, their oxidation to porphyrins by removal of six hydrogen atoms confers them *new* properties. They become intensely coloured displaying a strong light absorption band at about 400 nm (known as Soret band), plus four absorption bands in the visible region of the spectrum. Porphyrins fluoresce unless bounded to metals with the exception of Mg- and Zn-porphyrins, which fluoresce despite their metal content. This novel property - photosensitivity, turns them peril

to the cell. After absorbing light, they can transfer this energy to molecular oxygen producing reactive oxygen species, powerful cytotoxic molecules (Beale, 1999 and references within).

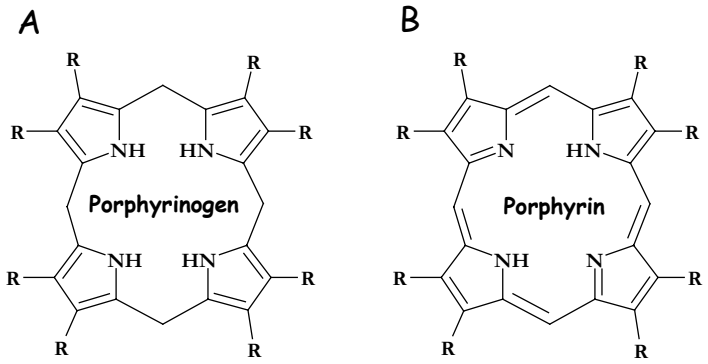

Figure 3 - Schematic representation of a porphyrinogen molecule (A) and the correspondent porphyrin (B). The letter R represents the side chains present in the different tetrapyrroles.

The regulation of the tetrapyrrole metabolism must guarantee a continuous flow of physiological intermediates to prevent the accumulation of these highly photoreactive molecules, and the consequent photodynamic cell damage (Mock and Grimm, 1997). Differences between the involved enzymes with regard to catalytic power, with low capacity steps positioned early in the catalytic chain, constitute, in addition to heme negative feedback, a control system for diminish substrate overloading. Transient multienzyme machineries would be physiologically favourable to assure an efficient substrate channelling throughout the pathway (Lash, 1991).

4.2 Chlorophyll and Heme Biosynthetic Pathway

Chlorophyll and heme are often described as the pigments of life. Chlorophyll plays an essential role in the photosynthetic process (harvesting of light and its subsequent conversion to chemical energy), and heme is an essential cofactor for oxygen and electron transport, for the reduction of nitrite and sulphite required in the biogenic cycles, for signalling and detoxification among other biological processes.

The enzymatic steps of their biosynthetic pathway have been highly conserved throughout evolution (Granik, 1950), (Wyckoff and Kushner, 1994). Because even the

common biosynthetic pathway for chlorophyll and heme is rather complex, it is convenient to approach it as four separated metabolic processes (schematically depicted in Figure 4). First, is the formation of ALA; second is the assembly of the tetrapyrrole macrocycle, uro-III; third is the modification of its side chains to generate protoporphyrinogen-IX (proto-IX) and its oxidation to protoporphyrin-IX; and fourth is the insertion of magnesium or iron into protoporphyrin-IX producing heme or branching to chlorophyll biosynthesis.

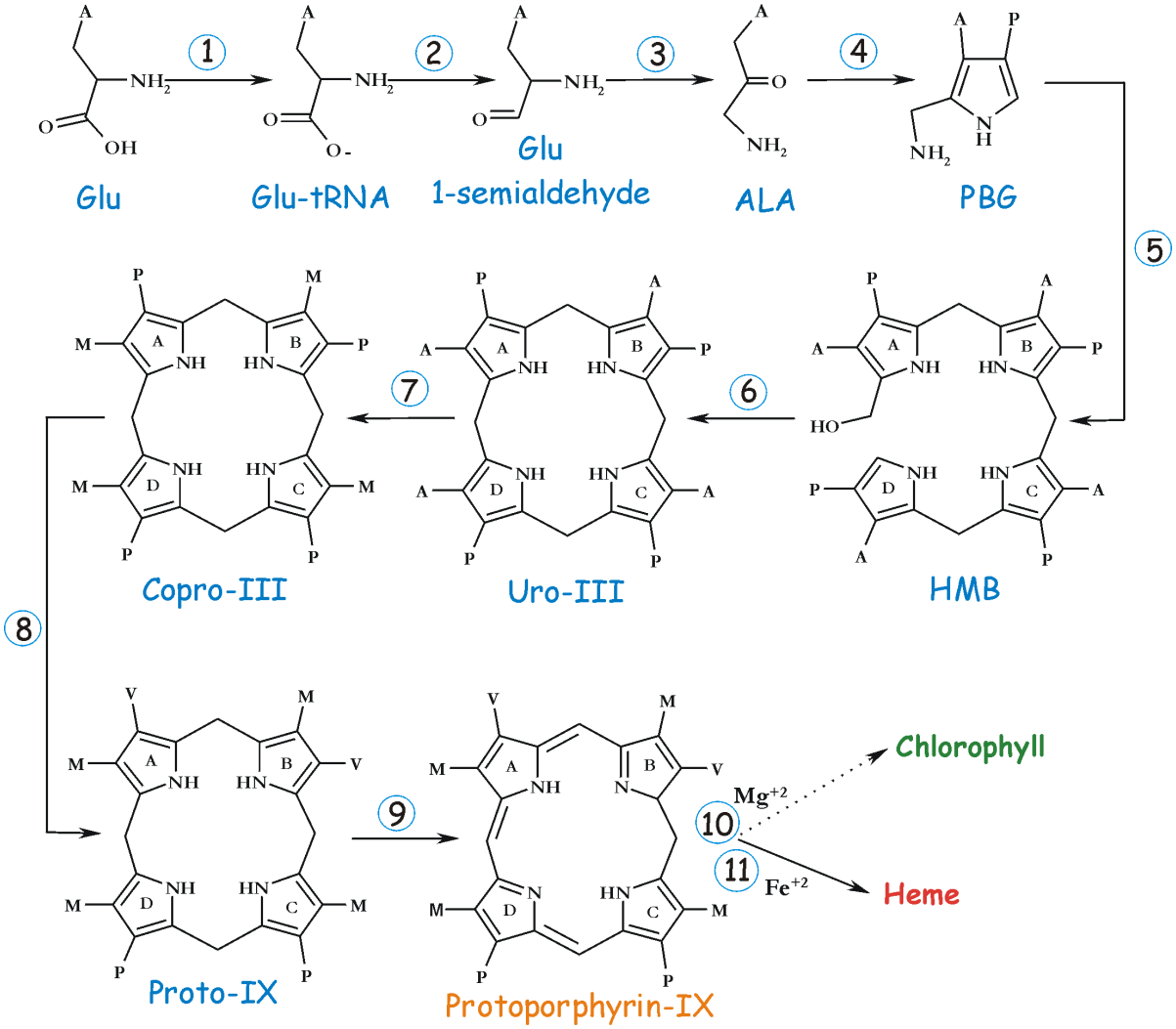

Figure 4 - Common enzymatic steps (1 to 9) for chlorophyll and heme biosynthesis. The abbreviations are: Glu, l-glutamate; Glu-tRNA, l-glutamyl-tRNA; Glu 1-semialdehyde, l-glutamate 1-semialdehyde; ALA, δ-aminolevulinic acid; PBG, porphobilinogen; HMB, hydroxymethylbilane; Uro-III, uroporphyrinogen-III; Copro-III, coproporphyrinogen-III; Proto-IX, protoporphyrinogen-IX; letters A, M, P and V designate acetate, methyl, propionate and vinyl groups, respectively. The enzymes that catalyse the individual numbered reactions are: (1) glutamyl-tRNA synthase; (2) glutamyl-tRNA reductase; (3) glutamate 1-semialdehyde aminotransferase; (4) porphybilinogen synthase; (5)

hydroxymethylbilane synthase; (6) uroporphyrinogen-III synthase; (7) uroporphyrinogen-III decarboxylase; (8) coproporphyrinogen-III oxidase; (9) protoporphyrinogen-IX oxidase; (10) magnesium chelatase; (11) iron chelatase. The last common precursor, protoporphyrin-IX is highlighted in orange.

In plants, chlorophyll synthesis is exclusively located in chloroplasts, whereas heme synthesis is found both in chloroplasts and mitochondria (last two enzymatic steps), probably due to the independent need for heme in both organelles (Jacobs and Jacobs, 1995). All of the enzymes involved from the beginning of the pathway to coproporphyrinogen-III oxidase, are restricted to the chloroplast. In contrast to the plant duality, heme is the single end product in mammalian cells, where the biosynthetic pathway is divided between two cellular compartments: the mitochondria (matrix and intermembrane spaces) and the cytoplasm (Kappas *et al.*, 1995). A similar organisation of the heme biosynthesis is found in prokaryotes. Here, the enzymes are localised in the cytoplasm or associated with the cytoplasmic membrane.

The substrate's aqueous solubility gradient along the pathway may explain the location of the corresponding enzymatic steps (Mauzerall, 1998). One begins with ionic, highly water soluble compounds, and one ends with a much less soluble heme molecule, and in the case of chlorophyll, an exclusively oil soluble molecule.

4.2.1 Biosynthesis of δ-Aminolevulinic Acid

Plants, algae and all other bacteria not belonging to the α proteobacterial group, including cyanobacteria, many photosynthetic bacteria, and archaea, form ALA by the sequential catalysis of three enzymes on the initial five-carbon precursor, glutamate (Beale and Castelfranco, 1973), (Meller *et al.*, 1975).

4.2.1.1 C_5 Pathway and the RNA Connection

The first step is the activation of glutamate to form glutamayl-tRNA. It seems to use the same enzyme as for protein synthesis, glutamyl-tRNA synthase (GluTS, EC 6.1.1.17) (Huang *et al.*, 1984) (Fig. 4, step 1). Like all aminoacyl-tRNA synthases, GluTS requires the cognate amino acid and tRNA as substrates, as well as energy from ATP hydrolysis. Its three dimensional structure ((Nureki *et al.*, 1995), PDB access code 1GLN) revealed that the N-

terminal domain fold is similar to the class I aminoacyl-transfer RNA synthase specific Rossman fold. In contrast, the C-terminal, responsible for the anticodon recognition displays a markedly distinct fold.

The next enzyme, glutamyl-tRNA reductase (GluTR, EC 1.2.1.-) is the least well understood enzyme of this pathway due to its high instability *in vitro*, low cellular abundance, and the need to provide a relatively unstable aminoacyl-tRNA substrate. The enzyme requires NADPH to reduce the tRNA-ligated α carboxyl group of glutamate to glutamate 1-semialdehyde (Kannangara, 1988) (Fig. 4, step 2).

Finally, glutamate 1-semialdehyde aminotransferase (GSA, EC 5.4.3.8) catalyses the rearrangement of the atoms of glutamate 1-semialdehyde to form the isomer, ALA (Fig. 4, step 3). The enzyme contains a pyridoxal phosphate or pyrodoxamine phosphate cofactor (Hoober *et al*., 1988). GSA is also structurally characterised ((Hennig *et al*., 1997), PBD code 2GSA). The enzyme has a dimeric structure with the two active sites situated at the subunit interfaces. The active sites seem to interact conformationally in that while one is in an open conformation that can accept substrate or release product, the other is in a close conformation that firmly binds the intermediate during the double transamination reaction.

Although each of the three reactions in the conversion of glutamate to ALA can occur independently, there is some preliminary evidence suggesting the enzymes may interact with each other (Jahn, 1992). A complex between GluTS and GluTR may facilitate the channelling of glutamyl-tRNA towards ALA biosynthesis and regulate competition with the protein synthesising apparatus.

4.2.2 Assembly of Uroporphyrinogen-III

Three sequentially working enzymes convert eight molecules of ALA to one molecule of uro-III, the first macrocycle tetrapyrrole precursor. These are the enzymatic steps common to all biologically relevant tetrapyrroles (see Fig. 2).

4.2.2.1 Porphybilinogen Formation

Porphobilinogen synthase (PBGS, EC 4.2.1.24, also known as ALA dehydratase) catalyses the asymmetric condensation of two ALA molecules to form the monopyrrole

porphybilinogen, PBG (Fig. 4, step 4). In this reaction, two identical molecules are combined to produce a product that is not a simple dimer, but a distinctly different molecule. The first ALA molecule to be bound is the one that contributes the propionate acid side chain of the product (Jordan and Seehra, 1980).

The enzyme's three-dimensional structure (Erskine *et al.*, 1997) revealed it to be a homooctamer, with all the eight active sites situated at the surface and at the interfaces of two subunits. Each substrate molecule is bound to the enzyme via a Schiff-base linked to a Lys residue. Despite an overall high sequence similarity, there are significant differences among the enzymes from different species with regard to the use of divalent cations for the catalytic essential and allosteric roles (Jaffe, 2000). There may be up to four specific divalent metal ion binding sites, each serving an unique function that can be alternatively filled by amino acids in some of the PBGs.

4.2.2.2 Formation and Cyclisation of Hydroxymethylbilane

Four molecules of PBG are next polymerised to yield the first macrocyclic precursor of all tetrapyrroles, uro-III. This complex reaction requires two enzymes acting in concert, Hydroxymethylbilane synthase (HMBS, EC 4.3.1.8, also known as PBG deaminase) and Uroporphyrinogen-III synthase (UROS, EC 4.2.1.75).

Formation of the Linear Tetrapyrrole HMB

HMBS condenses four PBG molecules to form the linear tetrapyrrole HMB (Fig. 4, step 5). In the absence of UROS, HMB spontaneously undergoes a non-enzymatically enclosure forming the non-physiological relevant end product uroporphyrinogen-I (uro-I). Although uro-I can be decarboxylated by uroporphyrinogen-III decarboxylase (UROD, see below), further metabolism cannot proceed because the following enzyme in the pathway, coproporphyrinogen-III oxidase (CPO, see below) is stereospecific for the isomer III.

The crystal structure of HMBS (Louie *et al.*, 1992) revealed a large active site cleft with a novel cofactor, a dipyrrolemethane molecule covalently attached to a cysteine residue. The cofactor acts as a primer onto which four PBGs are successively condensed, head to tail. During assembly of this chain the enzyme undergoes marked conformational changes. Once the pyrrole chain reaches a length of six units the last four units are clipped off to yield the product, leaving the holoenzyme ready to begin another enzymatic assembly. The precursor

for this cofactor appears to be the reaction product, HMB rather than its substrate, PBG (also used but at a much lower rate) (Shoolingin-Jordan *et al.*, 1996). Thus, HMBS can produce its own cofactor, catalyse PBG polymerisation and terminate the process when the chain is long enough.

Cyclisation of HMB

The cyclisation of HMB is catalysed by UROS (Fig. 4, step 6). This enzyme converts a regularly substituted liner tetramer into an unsymmetrical substituted cyclic tetramer. As mentioned above, free HMB rapidly cyclises spontaneously and irreversibly to form the non-physiological product uro-I unless UROS is present to direct its conversion to the correct isomer, uro-III. The reaction mechanism is unique because the terminal pyrrole ring D of the substrate undergoes a rearrangement that effectively "flips" it. This ring inversion involves a *spiro* intermediate (Crockett *et al.*, 1991).

UROS together with HMBS may form a complex that facilitates transfer of HMB between them (Rose *et al.*, 1988).

4.2.3 Formation of Protoporphyrin-IX

The three enzymes that sequentially convert uro-III to protoporphyrin-IX are responsible for transforming the former from a hydrophilic, poor metal binding, photochemically unreactive species into one that is hydrophobic, binds metal tightly, and is photochemically reactive ((Beale, 1999) and references within). The use of porphyrinogens rather than porphyirins in the earlier part of the pathway is advantageous to the organisms because the formers are much less photoreactive. Only at the last step, where the metal chelating properties of the prophyrin are needed, is the porphyrinogen convert to a porphyrin.

4.2.3.1 Multi-Decarboxylation of Uroporphyrinogen-III

Uroporphyrinogen-III decarboxyase (UROD, EC 4.1.1.37) catalyses the stepwise decarboxylation of all the four acetate side chains of uro-III to form coproporphyrinogen-III (copro-III) (Fig. 4, step 7). UROD appears to be the first decarboxylating enzyme without requirement for prosthetic groups or cofactors (de Verneuil *et al.*, 1983), (Straka and Kushner,

1983). While at higher substrate concentrations, the reactions occur randomly, under physiological conditions, the catalysis involves a stepwise decarboxylation. The carboxylate group at the acetate side chain from the asymmetric pyrrole ring D is removed first followed by a sequential decarboxylation reaction at rings A, B and C (Jackson *et al.*, 1976b), (Luo and Lim, 1993) (Fig. 5). For a correct positioning of ring A side chains, the first intermediate molecule has to flip by 180° around the axis parallel to the carbon atoms C_{10} and C_{20} (Akhtar, 1994). This obligatory displacement of the first reaction intermediate within the catalytic cleft constitutes probably the most challenging aspect of the UROD catalytic mechanism.

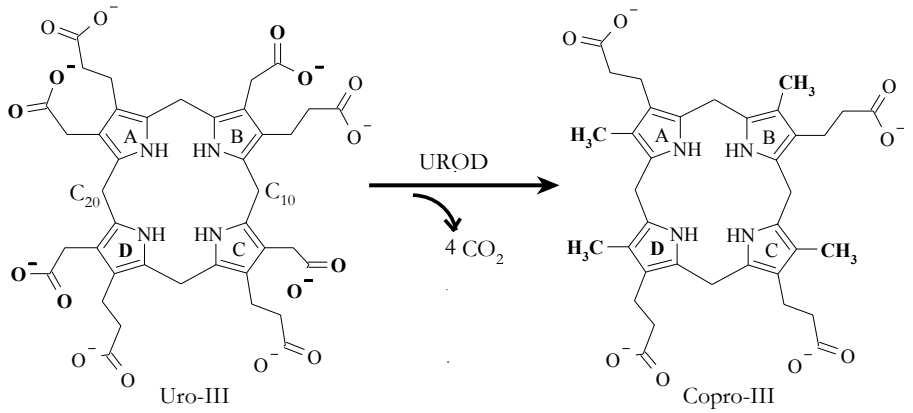

Figure 5 - Catalytic decarboxylation of uro-III to copro-III. The removed carboxylate groups from each acetate side chains are marked in bold. The sequence of the sequential reaction starts at the asymmetric ring D (in bold) and proceeds in a clockwise fashion trough rings A, B and C.

The enzyme catalyses the decarboxylation of all four possible uroporphyrinogen isomers. This wide substrate specificity suggests that the active site is flexible, enabling the enzyme to combine specificity with promiscuity ((Akhtar, 1994) and references within). Most decarboxylases utilise pyridoxal phosphate, thiamin pyrophosphate or biotin as cofactors. A reaction model independent of cofactor or prosthetic group has been proposed (Barnard and Akhtar, 1975). In this model, the pyrrole ring is protonated during the decarboxylation and acts as an electron sink, similar to the pyridine ring function in the pyridoxal phosphate cofactor. The protonation of the pyrrol ring requires the porphyrinogen conformation, which may explain the substrate specificity of UROD for uroporphyrinogens and not uroporphyrins.

Albeit extensive biochemical and site-directed mutagenesis studies allowed the identification of several residues critical for substrate binding and/or catalysis (de Verneuil *et*

al., 1983), (Straka and Kushner, 1983), (Kawanishi *et al*., 1983), (Felix and Brouillet, 1990), (Wyckoff *et al*., 1996) the number of catalytic sites per enzyme molecule remained controversial. Only recently, with the determination of the crystal structure from the homologous human enzyme (Whitby *et al*., 1998) it was possible to identify the putative substrate binding cleft, thus confirming the presence of one single catalytic site per molecule (Elder and Roberts, 1995). However, the sequence of protein-substrate interactions during the catalysis remained unknown.

UROD has been the object of considerable attention since its deficient activity is associated with porphyria cutanea tarda (PCT, see section *3.3 Impaired Heme Biosynthesis and Porphyrias*). Whereas the human UROD has been extensively studied, culminating in the recent determination of its crystal structure (Whitby *et al*., 1998), the plant enzyme has been relatively little studied.

Tobacco UROD is located in the stroma of the chloroplast (Mock *et al*., 1995), whereas in mammals, yeast and some bacteria it is cytosolic (Jacobs and Jacobs, 1993). The newly synthesised enzyme has a molecular mass of 43 kDa corresponding to the mature protein with 39 kDa plus an N-terminal signal peptid for the chloroplast. Tobacco UROD displays 33% overall similarity to prokaryotic and eukaryotic homologous proteins (Kruse *et al*., 1995a).

The necrotic phenotype of transgenic tobacco plants expressing UROD antisense RNA is analogous to human PCT (Kruse *et al*., 1997), (Hu *et al*., 1998) indicating that UROD deficiency generally leads to cellular photosensitization by accumulating uroporphyrin. The cellular responses upon porphyric stress interfere with the signal transduction pathway triggered by pathogen infection. Moreover, the phenotype of reduced UROD activity resembles accumulation of protoporphyrin-IX by inhibition of protoporphyrinogen-IX oxidase (see below) (Lehnen *et al*., 1990), a target protein in herbicide treatment.

Annually, 2.4 x 10^8 tons of biomass are produced alone by chlorophyll biogenesis, and its natural degradation has strong economic implications in several sectors including crop productivity, food industry and tourism. Apart from the economic interest due to potential applications in agriculture and biotechnology such as design of environmentally safe herbicides, the study of plants and their enzymes may contribute to the development of both effective treatments for porphyria disorders and crop plants exhibiting a broad pathogen resistance spectrum.

Recently, a novel pathway of heme biosynthesis has been described in the obligate anaerobe *Desulfovibrio vulgaris* Miyazaki F (Ishida *et al.*, 1998). The conversion of uro-III into copro-III is not directly catalysed by the sequential decarboxylation with UROD, but involves two enzymes. The evolutionary origin of those enzymes and their replacement by a single enzyme in *younger* organisms strengths the interest in the biochemical and structural characterisation of UROD from prokaryotic and eukaryotic organisms.

4.2.3.2 Oxidative Decarboxylation of Coproporhyrinogen-III

Coproporphyrinogen-III oxidase (CPO, EC 1.3.3.3) is one of the least understood enzymes from the tetrapyrrole biosynthetic pathway. CPO catalyses, in two sequential steps the oxidative decarboxylation at two specific propionate sides chains of copro-III to yield protoporphyrinogen-IX (proto-IX) (Fig. 4, step 8). A proposed mechanism involves pyrrolic N-assisted removal of single hydrogen atoms as hydride ions from the β-carbons of the propionate groups, with no apparent involvement of its α-protons (Akhtar *et al.*, 1976), (Seehra *et al.*, 1983). The reaction starts at ring A and proceeds to ring B (Fig. 6).

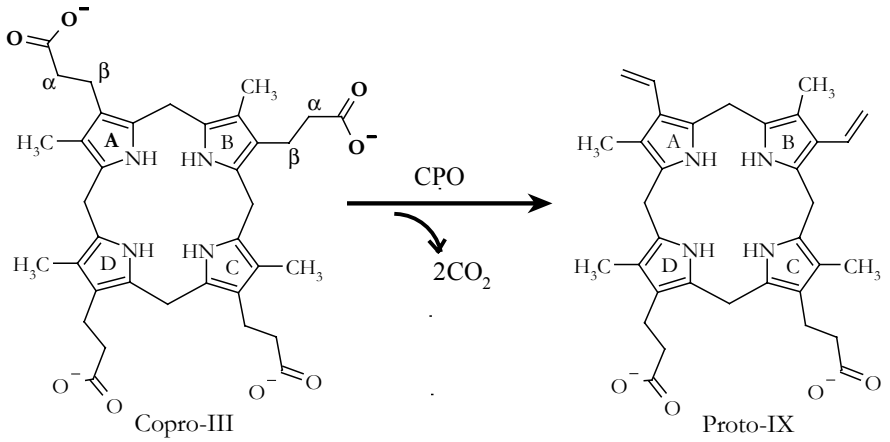

Figure 6 - Catalytic oxidative decarboxylation of copro-III to proto-IX. The removed carboxylate groups from two propionate side chains are marked in bold. The sequence of the sequential reaction starts at ring A (in bold) and proceeds in a clockwise fashion to ring B. The symbols α and β indicate carbon atoms from the propionate side chain.

Whereas molecular oxygen is the electron acceptor in aerobic systems, facultative anaerobes can carry out the reaction in the absence of oxygen by way of a different enzyme in the presence of ATP, $NADP^+$, NADH, Mg^{2+} and methionine (Tait, 1972), (Poulson and

Polglase, 1974). For instance, the facultative organism *E. coli* has both an oxygen-dependent (hemF) and an oxygen-independent CPO (hemN) (Troup *et al.*, 1995).

The enzymatic catalysis of oxygen-dependent CPO had been the subject to controversial discussion. Whereas copper-dependent catalysis was reported for the mouse enzyme (Kohno *et al.*, 1996), no metal dependence was identified for the human enzyme expressed in *E. coli* (Medlock and Dailey, 1996), (Martasek *et al.*, 1997) or any other characerised CPO (Sorianello *et al.*, 2000 and references within). Moreover, the *C. reinhardtii* enzyme displays an elevated activity in copper deficient cells (Hill and Merchant, 1995). All characterised oxygen-dependent CPOs indicate a dimeric form in solution (Sorianello *et al.*, 2000 and references within). In mammals, CPO is associated with the mitochondrial inner membrane, opposite to bacterial CPO located in the cytoplasm. In plants, CPO is located in the chloroplasts' stroma (Beale, 1999).

Deficiency of CPO in humans is responsible for hereditary coproporphyria (HCP), an autosomal dominant disease (see section *3.3 Impaired Heme Biosynthesis and Porphyrias*). Symptoms of this disease include neurological disturbances and cutaneous photosensitivity (Kappas *et al.*, 1995). Albeit genetic and biochemical studies identified several residues ((Lash *et al.*, 2001) and references within) possibly involved in catalysis, structural information is required for a fully understanding of this pathology.

The degree of primary sequence conservation (30 % overall identity) displayed by the oxygen-dependent CPOs family suggests a similar structural fold for its members (Kruse *et al.*, 1995b). In particular, the *E. coli* enzyme displays more than 40 % overall identity with the human counterpart, making this protein a good model for biochemical and structural analyses. Additional to its contribution to a better understanding of the human metabolic disorder HCP, the structure determination of this representative member will assess the new three-dimensional fold predicted for this enzyme family.

4.2.3.3 Oxidation of Protoporphyrinogen-IX

The last common step in the chlorophyll and heme biosynthetic pathway is the oxidation of proto-IX to protoporphyrin-IX, catalysed by protoporphyrinogen-IX oxidase (PPO, EC 1.3.3.4; Fig. 4, step 9). It is at this step that the synthesis switches from colourless, flexible unconjugated intermediates to coloured, conjugated, and relatively rigid planar structures (Mauzerall, 1998). The overall reaction involves the removal of six hydrogen atoms

from the proto-IX nucleus. The catalysis is still unknown but labelling studies have shown that the hydrogen removal is stereoselective (Akhtar, 1994). PPO acts specifically on proto-IX, not catalysing the oxidation of uro-I, copro-I or copro–III.

Unlike all of the previous enzymatic steps, which in plants are located exclusively in the chloroplasts, PPO is found in both chloroplast and mitochondria organelles (Jacobs and Jacobs, 1987). The dual localisation in plants is accentuated by a rather low degree of amino acid conservation (27 % identical) (Lermontova *et al*., 1997).

In plants, mammals and some bacteria, PPO has an absolute requirement for oxygen as electron acceptor and utilises FAD as cofactor. However, the respiratory chain can function as the electron acceptor in anaerobically grown *E. coli* (whose PPO does not need FAD) and presumably also in anaerobic photosynthetic bacteria (Klemm and Barton, 1987). Similar to the oxygen dependence/independence duality observed for the previous enzymatic step, the anaerobic reaction appears to be catalysed by a different enzyme, but notably, these two enzymes have not been observed in the same organism.

Defective or inhibited PPO is relevant in nature. In humans, inherited defects result in varigate porphyria (see section *3.3 Impaired Heme Biosynthesis and Porphyrias*), and plant PPO is of agricultural interest. The enzyme is the target of a class of herbicides that inhibit it and cause a massive build-up of cellular proto-IX (Lehnen *et al*., 1990). This compound diffuses to the cell membrane where after being nonspecifically oxidised can cause photodynamic damage and cell death.

4.2.4 Metal Insertion into Protoporphyrin-IX

The branching point of chlorophyll and heme is at the level of protoporphyrin-IX utilisation for metal ion chelation. Insertion of magnesium into protoporhyrin-IX by Mg-chelatase (EC 4.99.1.-) (Fig. 4, step 10) continues to chlorophyll biosynthesis. In heme biosynthesis, a ferrous ion (Fe^{+2}) is inserted into the tetrapyrrole ring by the enzyme ferrochelatase (EC 4.99.1.1) (Fig. 4, step 11) generating heme.

Unlike the previous enzymatic steps, which utilise porphyrinogens, these two chelatases utilise protoporphyrin-IX (oxidised proto-IX) as substrate. Albeit catalysing comparable reactions, both enzymes share neither structural nor catalytic similarities (Beale, 1999).

4.2.4.1 Fe^{+2} Chelation to form Heme

The reaction proceeds spontaneously and reversibly in the presence of protoporphyrin-IX and ferrous iron, without the involvement of ATP or other energy sources (Loeb, 1995).

In most organisms, ferrochelatase is tightly bound to membranes, but a few bacterial enzymes are soluble proteins. The sequence homology is less than 10 % among all known ferrochelatases (Ferreira *et al.*, 1995). Eukaryotic enzymes possess a C-terminal extension, absence in most bacterial counterparts. Additionally, a [2Fe-2S] cluster is present in the enzymes of higher animals, but not in plants or yeast (Dailey *et al.*, 2000). The crystal structure of ferrochelatase from *B. subtilis* and human have been reported ((Al-Karadaghi *et al.*, 1997) and (Wu *et al.*, 2001), PDB access codes: 1AK1 and 1HRK, respectively). In human ferroclelatase, three from the four cysteine residues, responsible for the cluster binding are located in the C-terminal extension, which is extensively involved in the dimer interface. The comparison of both bacterial and mammal structures suggests that the cluster plays an indirect role in dimerisation of animals ferrochelatases. In line with this, ferrochelatases from species without the C-terminal segment are monomeric (Dailey *et al.*, 1994).

4.2.4.2 Mg^{+2} Chelation in Route to Chlorophyll

In all photosynthetic organisms studied to date, Mg-chelatase is a three-component enzyme (ChlD, ChlH and ChlI) (Jensen *et al.*, 1996). The reaction takes place in two steps, with an ATP dependent activation followed by the ATP independent magnesium chelation ((Beale, 1999) and references within). Chemically, insertion of Mg^{2+} into the protoporhyrin-IX is very difficult, in part because of the difficulty of removing water molecules coordinated to the ion. The role of ATP may be to provide the energy needed to remove these water molecules, possibly by consuming them during the hydrolysis of ATP.

Magnesium, in addition to its role as substrate, influences the association of the enzyme components with the envelope membrane of chloroplast (they become soluble in its absence) (Gibson *et al.*, 1996), (Kannangara *et al.*, 1997). Preliminary results suggest that the H subunit binds protoporphyrin-IX (Grafe *et al.*, 1999), and that both D and I subunits bind ATP, possibly one for activation and the other for catalysis (Petersen *et al.*, 1999). Curiously, the enzyme components have significant similarity to Co- and Ni-chelatases, responsible for the last steps of $VitB_{12}$ and cofactor F_{430} biosynthesis (Walker and Willows, 1997). It is not

clear whether all three subunits need to be present simultaneously for activity, as well as which is the optimal stoichiometry for the three components. The crystallisation of ChlI has been reported (Willows *et al*., 1999).

Five additional enzymes sequentially convert magnesium protoporphyrin-IX into chlorophyll *a*. First is the formation of the isocyclic (*fifth*) ring (two enzymes involved). Second is the reduction of the vinyl group from ring B. Third is the reduction of ring D. Finally, the addition of a long chain fatty alcohol (geranyl geranyl or phytyl) result in the formation of chlorophyll *a*, the biologically functional end product (Grimm, 1998).

4.3 Impaired Heme Biosynthesis and Porphyrias

Porphyrias are a heterogeneous group of inherited and acquired metabolic disorders characterised by an abnormal heme biosynthesis (Wyckoff and Kushner, 1994). There are eight enzymes involved in this pathway and, except for the first enzyme (ALAS) deficiencies in their catalytic activity are associated with the various forms of porphyria (Table 1) (Sassa and Kappas, 2000) (and references within).

Table 1

Enzymatic defects in human heme biosynthesis and Porphyrias

Enzyme	Type of Porphyria	Classification
PBGS	ADP[1]	Neurovisceral
PBGD	AIP[2]	Neurovisceral
UROS	CEP[3]	Photosensitivity
UROD	PCT[4a], HEP[4b]	Photosensitivity & Liver damage
CPO	HCP[5]	Neurovisceral & Photosensitivity
PPO	VP[6]	Neurovisceral & Photosensitivity
Fe-Chelatase	EPP[7]	Photosensitivity & Liver damage

[1]ALAD Deficiency Porphyria; [2]Acute Intermittent Porphyria; [3]Congenital Erythropoietic Porphyria; [4a]Porphyria Cutanea Tarda; [4b]Hepatoerythropoietic Porphyria; [5]Hereditary Coproporphyria; [6]Varigate Porphyria and [7]Erythropoietic Protopoporphyria.

These metabolic disorders can be classified as either photosensitive or neurological, depending on the type of symptoms. Alternatively, they can be classified as either hepatic or erythropoietic, depending on the major site of expression of the specific enzymatic defect, (Kappas *et al*., 1995). The neurologic manifestations occur when there is overproduction and excretion of ALA and PBG. Cutaneous photosensitivity is generally restricted to light exposed areas and results from the fluorescent properties of the porphyrins, which accumulate in cellular tissues. When porphyrins together with ALA and PBG are produced in excess, both cutaneous and neurologic symptoms are found.

Porphyria cutanea tarda (PCT), the most prevalent of human porphyrias afflicts roughly one of every 5,000 people, and is normally associated with hemochromatosis (Elder and Worwood, 1998). Alcohol, estrogens, iron overload and hepatitis viruses may precipitate this metabolic disorder. Patients with PCT suffer liver damage, a possible increase in facial hair growth, fragile skin and fluid-filled blisters on the face, arms, hands and other skin exposed to sun (Fig. 7).

Figure 7 – Hand of a PCT patient.

A rare variant, Hepatoerythropoietic porphyria (HEP), associated with homozygous deficiency is characterised by severe photosensitivity without frank liver involvement. A third variant, toxic PCT is associated with exposure to halogenated aromatic hydrocarbons. Their inhibitory mechanism is unknown, but animal models have suggested that both iron and the induction of specific isoenzymes of Cytochrome P-450 are involved (Wyckoff and Kushner, 1994).

But porphyrins do not have only a dark side. Their photosensitivity can be successfully explored for medical applications such as photodynamic therapy in cancer

treatment (Kessel, 1984). Their discrimination between normal and malignant cells with a specific and much longer retention by the latter, allows both the detection and then selective destruction of the tumor with only limited or negligible damage to surrounding normal cells.

5 Experimental Procedures

5.1 Molecular Biology

5.1.1 *E. coli* Oxygen-dependent Coproporphyrinogen-III Oxidase

5.1.1.1 Cloning

The expression vector for Oxygen-dependent coproporphyrinogen-III oxidase (CPO) from *E. coli* was kindly provided by Holger Dobbek and Oliver Einsle. The *hem*F gene was cloned in the expression vector pET-22b(+) (Novagen) using restriction enzymes *Nde*I and *Xho*I. The vector harboured a C-terminal His_6-tag.

The *E. coli* strain BL21 (DE3) was used for transformation purposes during the cloning of CPO. The respective relevant genotype was:

- BL21 (DE3): F^- *ompT* $hsdS_B$ ($r_B^- m_B^-$) *gal dcm* (DE3)

Bacteria were grown at 37 °C in Luria-Bertani (LB) medium (Sambrook *et al.*, 1989). For selection of transformands, antibiotic resistance was performed by supplementing the medium with ampicillin to a concentration of 100 μg ml^{-1}. Transformation was carried out by electroporation (Sambrook *et al.*, 1989).

5.1.1.2 Recombinant Homologous Over-Expression

The *E. coli* strains BL21 (DE3) and B834 (DE3) (Novagen) were used for over-expression of CPO and Selenomethionine substituted CPO (SeMet-CPO), respectively. The relevant genotype from B834 (DE3) was:

- B834 (DE3): F^- *ompT* $hsdS_B$ ($r_B^- m_B^-$) *gal dcm met* (DE3)

Pre-cultures grown in LB medium were used to inoculate freshly prepared twice concentrated LB medium or New Minimal (NM) medium containing 0.3 mM seleno-DL-methionine (Budisa *et al.*, 1995) for expression of recombinant CPO and SeMet-CPO,

respectively. The media were supplemented with ampicillin (100 μg ml^{-1}) for antibiotic resistance selection. Induction was performed with IPTG (1 mM).

For large-scale purification purposes, glucose (1% (w/v)) was added to the pre-cultures to diminish expression leakage, allowing a higher cell mass production prior to induce the expression of the recombinant proteins.

5.2 Protein Biochemistry

Unless specifically mentioned, standard techniques and materials were used.

Protein samples were handled on ice and frozen in liquid nitrogen for long term storage (-20 and -80 °C). Amicon Ultrafiltration kit and Centricons (Amicon), and Ultrafee (Millipore) were used to concentrate protein solutions, and protein's buffer exchange was carried out on NAP gravity flow columns (Pharmacia) or using Centricons (Amicon). Several methods were used to characterise the purified proteins:

- Dynamic light scattering (DLS) measurements were performed at 20 °C using a DynaPro-801TC (Protein Solutions);
- Electron-spray mass spectometry (ES-MS) was performed using a SCIEX API165 spectometer (Perkin Elmer);
- Sedimentation equilibrium was done at 20 °C using a Beckman Optima XL-I analytical ultracentrifuge;
- Size exclusion chromatography was performed on a SMART™ FPLC system (Pharmacia) with Superdex-75 PC 3.2/30 and Superose-12 PC 3.2/30 columns. Column calibration was performed with globular protein size standards (Fluka and Biorad);
- SDS-PAGE (10 - 12.5 %) was performed according to Laemmli (Laemmli, 1970) on a BioRad system (BioRad). Gels were stained with Coomassie brillant blue G-250 or silver (Heukeshoven, 1985); Native-PAGE was performed with pre-casted 8 - 25 % gradient gels using the Phast System™ (Pharmacia);
- UV/Visible, Fluorescence and CD spectroscopy were performed using a Lambda 17 UV/Vis (Perkin Elmer), a LS 50B Luminescence (Perkin Elmer) and a Jobin Yvon (Division D'instruments, SA.) spectrometers, respectively.

5.2.1 Tobacco Uroporphyrinogen-III Decarboxylase

5.2.1.1 Assessment of Homogeneity and Oligomeric State in Solution

The recombinant mature tobacco UROD (Val1–Tyr352) (see Figure x for amino acid sequence) was expressed and purified as described elsewhere (Mock *et al.*, 1995).

SDS-PAGE and N-terminal peptide sequencing assessed its purity and integrity. The protein concentration was determined by absorption spectroscopy using a molar extinction coefficient of 35590 M^{-1} cm^{-1} at 280 nm (Protparam tool from Expasy: http://www.expasy.org/tools/protparam).

The homogeneity and oligomeric state of tobacco UROD in solution was analysed by DLS, sedimentation velocity and sedimentation equilibrium. The partial specific volume of the protein and the density of the solvent were estimated according to published procedures (Lane *et al.*, 1992).

5.2.2 *E. coli* Oxygen-dependent Coproporphyrinogen-III Oxidase

5.2.2.1 Protein Over-Expression

Cells from an overnight culture grown in LB medium supplemented with 100 μg ml^{-1} ampicillin (selective LB medium) were used to inoculate 4 litres of twice concentrated selective LB medium (freshly prepared), and the cell culture was grown at 37 °C to an optical density (OD_{600nm}) of 0.6 - 1.0. Following induction with 1 mM IPTG, the culture was grown for additional 3 h and then harvested at an OD_{600nm} of 1.5 - 2.0 by centrifugation at 4200 rpm, 4°C for 25min.

An identical protocol was used for expressing SeMet-CPO. Five litres of NM medium, supplemented with 0.3 mM seleno-DL-methionine and 100 μg ml^{-1} ampicillin were inoculated with a 50 ml overnight culture grown in selective LB medium.

5.2.2.2 Large Scale Purification

Throughout the purification steps, the protein solutions were always handle at 4 °C with the exception of the Ni-NTA column (Qiagen) step for CPO, performed at 15 °C.

Cell pellet was resuspended at 10 ml per culture litre in lysis buffer (50 mM Tris/HCl pH 8.0, 300 mM NaCl, 10 mM Imidazol) containing 1 mg ml^{-1} lysozyme and EDTA-free protease inhibitor cocktail (Roche). Cells were disrupted by sonification and cell debris was removed by centrifugation at 18000 rpm for 30 min. The supernatent was loaded on a Ni-NTA column (Qiagen) previously equilibrated in lysis buffer. The column was washed following manufacturer instructions and the protein was eluted with a 200 - 400 mM Imidazol gradient. Collected fractions were analysed by SDS-PAGE and UV/Visible.

In the case of CPO, the pooled fractions were concentrated in 10 mM MES/NaOH pH 6.5, aliquoted, shock frozen in liquid nitrogen and stored at -80 °C. For SeMet-CPO, an additional gel filtration step was performed. The protein containing fractions eluted from the Ni-NTA column were concentrated and loaded on a High-Load 26/60 Superdex-75 column (Pharmacia) previously equilibrated in PBS buffer (1 mM KH_2PO_4, 10 mM Na_2HPO_4, 137 mM NaCl, 2.7 mM KCl, pH 7.4). Eluted protein was concentrated in PBS, 2 mM DTT, aliquoted, shock frozen in liquid nitrogen and stored at -80 °C. Protein concentration was determined by absorption spectroscopy at 280nm using an extinction coefficient of 62280 M^{-1} cm^{-1} (Protparam tool from Expasy: http://www.expasy.org/tools/protparam).

Protein purity and structural integrity were confirmed by N-terminal peptide, SDS-PAGE sequencing, ES-MS and CD spectroscopy. Complete Seleno-methionine incorporation was checked by ES-MS. Metal analysis was performed by ICP-AES (BITÖK, Bayreuth, Germany).

5.2.2.3 Identification of the co-purified Porphyrin

UV/Visible in the range 650 – 220nm and Fluorescence spectra from purified CPO indicated the present of a porphyrin compound. For Fluorescence spectra, excitation wavelength of 666 nm and emission range of 600 – 350 nm were set.

A chemical characterisation was performed with an organic phase extraction from 100 µl of protein solution (10 mg ml^{-1} in 10 mM MES/NaOH pH 6.5) in a glass vial. Methanol (400 µl) was added to the protein solution, followed by addition of chloroform (100 µl) and bi-deionised water (300 µl). The resulting solution was strongly shacked and left to settle overnight at 4 °C. ES-MS was performed from both organic and aqueous phases.

5.2.2.4 Activity Assay

The enzyme activity was measured by a fluorometric assay according to Labbe (Labbe *et al.*, 1985). Substrate coproporphyrinogen-III was freshly prepared by reducing coproporphyrin-III dihydrochloride (Porphyrin Products) with 3 % sodium amalgam under dim light inside an anaerobic chamber. Coproporphyrinogen-III formation was quantitated spectrophotometrically in 0.1 N HCl at 400 nm using an extinction coefficient of 489 mM^{-1} cm^{-1}. Protein aliquots (~ 130 μg ml^{-1} in PBS, 2 mDTT) were incubated with 8 μM coproporphyrinogen-III at 37 °C in the dark for 30 min in the absence and presence of a three fold excess of protoporphyrinogen-Ix oxidase (kindly supplied by M. Koch). The reaction was stopped by adding 1 ml of 10 % HCl and furhter exposed to light for 1 hour in ice for assays performed in the absence of protoporphyrinogen-IX oxidase. The formation of protoporphyrin-IX was monitored fluorometrically with excitation at 408 nm (slit at 2.5 nm) and emission wavelengths at 632 nm (slit at 20 nm). The amount of product formed was determined using a calibration curve of Protoporphyrin-IX fluorescence standard (Porphyrin Products).

5.2.2.5 Identification of Oligomeric State in Solution

The homogeneity and oligomeric state of CPO in solution was analysed by dynamic light scattering, sedimentation velocity and equilibrium, size exclusion chromatography and gradient native PAGE.

Size exclusion chromatography was performed on a SMART™ FPLC system (Pharmacia) with Superose-12 PC 3.2/30 column. Column calibration was performed with globular protein size standards (Fluka and Biorad). Protein elution was carried out at 50 μl min^{-1} using the following buffers:

- 10 mM MES/NaOH pH 6.5 (buffer A);
- 150, 300 and 500 mM sodium chloride, 10 mM MES/NaOH pH 6.5 (buffers B, C and D, respectively);
- PBS (1 mM KH_2PO_4, 10 mM Na_2HPO_4, 137 mm NaCl, 2.7 mM KCl, pH 7.4) (buffer E);
- PBS with 2 mM DTT and 10 mM DTT (buffers E and F, respectively).

For dynamic light scattering (DLS) measurements, protein samples at approximately 1 and 5 mg ml^{-1} (in buffers A, D, E and F) were filtered according to the manufacture's

instructions and 25 to 30 readings were taken per sample. Molecular mass was calculated assuming a globular conformation model using the software provided by the manufacturer.

Native-PAGE analysis was performed with protein samples at a concentration of approximately 0.25 and 1 mg ml^{-1} in pre-casted 8 to 25 % gradient gels (Pharmacia).

5.3 Protein Crystallography

A detailed discussion of X-ray diffraction techniques for determination of macromolecular structures is beyond the scope of the present work and can be found in a number of textbooks ((Blundell and Johnson, 1976),(Drenth, 1994), (Glusker *et al.*, 1994); (McRee, 1993), (Methods in Enzymology, vol. 276, Part A, 1997).

Crystallisation trials were carried out using standard material and solutions, home made and sparse-matrix screens (Hampton Research). Buffers of low ionic strength were used, most commonly 10 mM MES/NaOH pH 6.5, 10 mM Tris/HCl pH 7 or 0.07 diluted PBS pH 7.4.

5.3.1 Tobacco Uroporphyrinogen-III Decarboxylase

5.3.1.1 Crystal Growth, Cryoprotection and Data Collection

Prior to crystallisation, the protein was concentrated to approximately 5 mg ml^{-1} using a Centricon concentrator (30 kDa cut-off) in 10 mM Tris/HCl pH 7.

The initial crystallisation trials were carried out with a grid screen of ammonium sulphate *versus* pH 9-12 (solutions buffered with 250 mM sodium borate/boric acid). The droplets were made by mixing 3 µl of protein solution with 1 µl of reservoir solution (1 ml) using the hanging drop vapour diffusion method at 20 °C. When combining a diluted protein with a double drop volume, small crystals were obtained in 1.2 M ammonium sulphate pH 9.6 reaching dimensions of roughly 400 x 250 x 50 μm^3 after 18 months.

The diffraction quality of the crystals was tested on an in-house imaging plate detector (MAR Research) coupled to a RU-200 rotating anode X-ray generator (Rigaku) producing Cu $K\alpha$ radiation with a wavelength of 1.5418 Å.

For data collection using synchrotron radiation, the crystals were harvested with cryoloops of the same dimensions, shortly immersed in cryoprotectant buffer (1.5 M ammonium sulphate, 100 mM MOPS at pH 7.5 plus 10 % (v/v) of 2,3-R,R-butanodiol) and flash cooled in a nitrogen stream at -180 °C (Oxford Cryosystems).

The crystals belong to space group P622, with unit cell constants of a = b = 158.44 Å and c = 67.68 Å. There is one molecule per asymmetric unit of the unit cell and the Matthews coefficient (Matthews, 1968) of V_m = 3.14 $Å^3$/Da correspond to a solvent content of 61%. Data were evaluated using DENZO and SCALEPACK (Otwinowski and Minor, 1996).

Co-crystallisation trials in the presence of inhibitors (uroporphyrin-III, coproporphyrin-III and mesoporphyrin-IX, purchased from Porphyrin Products) were performed by adding 0.1 µl from inhibitor solutions (~ 100 µM) to the droplets. For soaking experiments, crystals were transferred into pre-equilibrated droplets additionally containing one of the inhibitors (~ 10 µM final concentration). To avoid photoactivation of the porphyrin compounds, all trials in the presence of inhibitors were kept in the dark. The crystallisation plates where involved in aluminium foil and placed inside hermetic (*styropor*) boxes.

5.3.1.2 Structure Determination

The long period necessary to growth crystals of tobacco UROD suitable for X-ray diffraction (18 months) hindered the determination of its crystal structure using experimental phases. The availability of the three dimensional structure from the human homologous protein (Whitby *et al.*, 1998) made possible the determination of the tobacco UROD crystal structure by Patterson search using the program AMoRe (Navaza, 1994).

Density modification with DM (CCP4) (Collaborative Computational Project No. 4, 1994, and simulated annealing with CNS (Brünger *et al.*, 1998) helped the initial density interpretation and model building in MAIN (Turk, 1992) using ($2F_{obs}$ - F_{cal}) and (F_{obs} - F_{cal}) electron density maps. The initial model was then improved by iterative rounds of model building and refinement using overall anisotropic *B*-factor correction for *Fobs*, torsion angle molecular dynamics, bulk solvent correction, and maximum likelihood targets for positional

and individual temperature-factors refinement using CNS. In the final stages of refinement, solvent molecules and sulphate ions were built in (F_{obs} - F_{cal}) maps with 2.5-3.0 and 5.0 σ contouring level, respectively.

5.3.1.3 Modelling of Substrate Complexes for Tobacco and Human enzymes

Molecular modelling was performed using the program package InsightII (Version 98.0; MSI, Los Angeles, USA). The monomers of the refined crystal structures of human and tobacco UROD were chosen as starting point for the docking and energy minimisation of the substrate enzyme complexes. In the absence of structural information from the physiological substrate, uro-III, the crystal structure of a similar compound, uroporphyrinogen-octanitrile (type-I) tetrahydrofuran solvate (Lehmann *et al.*, 1997) was modified to uro-III using the module Builder. The substrate molecule was positioned in the active site using modules Builder and Docking with the acetate side chains of pyrrole rings D and A in hydrogen bonding distances to the carboxylic group of Asp86 (human), or Asp82 (tobacco) and the hydroxyl group of Tyr164 (human), or Tyr159 (tobacco), respectively. The Consistent Valence Force field (CVFF) was used for energy minimisation with Discover3 and 1000 minimisation steps were run. The protein and substrate molecules were simultaneously minimised.

5.3.1.4 Structural Analysis and Graphical Representation

Secondary structure assignment and quality assessments of the refined model were done with PROCHECK (Laskowski *et al.*, 1993), and superposition of tobacco and human monomers and dimers was performed with the program Swiss PDB Viewer (Guex and Peitsch, 1996).

The interactions at the crystallographic dimer interface were analysed with the Protein-Protein Interaction Server (http://www.biochem.ucl.ac.uk/bsm/PP/server). Accessibility calculations were done with GRASP (Nicholls *et al.*, 1993) and NACCESS (Hubbard *et al.*, 1991).

Illustrations of structures were prepared using Bobscript (Esnouf, 1997), Raster3D (Merrit and Bacon, 1997), Swiss-PdbViwer (Guex and Peitsch, 1996) and POVRay™. Surface representations were prepared with GRASP (Nicholls *et al.*, 1993) and Swiss-PdbViwer (Guex and Peitsch, 1996). Enzymatic reaction schemes were produced with ISISDRAW™, and the

amino acid sequence alignment was generated using the EMBL homology search tool Fasta3 (http:/www.ebi.ac.uk/fasta3/) and further modified.

5.3.2 *E. coli* Oxygen-dependent Coproporphyrinogen-III Oxidase

Initial crystallisation trials with CPO were carried out at 4 and 20 °C using the sitting drop vapour diffusion method. The droplets contained 2 µl of protein solution (5 mg ml^{-1} in 10 mM MES/NaOH pH 6.5) plus 2 µl of reservoir solution (300 µl). The crystallisation plates were kept in the dark.

Within few days needle bundles appeared at 20 °C in 200 mM ammonium acetate, 10 mM magnesium acetate, 50 mM sodium cacodylate/NaOH pH 6.5, 30 % (w/v) PEG 8K. The addition of 0.4 µl xylitol (30 % (w/v)) to the droplets improved the crystal growth and morphology resulting in thin long plates but with a common origin. Microseeding was next performed in an attempt to improve the crystal habit and size. For this, thin plates were cut from plate aggregates, extensively washed in reservoir solution and finely crashed into small microcrystals (seeds). These seeds were then added to pre-equilibrated protein drops, and the composition and concentration of the reservoir constituents was varied. The best seeding conditions obtained were:

- 0.1 M ammonium acetate, 10 mM magnesium acetate, 28 % PEG 8K, pH 6.5 (50 mM sodium cacodylate/NaOH), 2.7 % xylitol (addition of 4 µl to the droplets),
- 0.2 M ammonium acetate, 10 mM magnesium acetate, 28 % PEG 8K, pH 6.0 (50 mM sodium cacodylate/NaOH), 2.7 % xylitol (addition of 0.4 µl to the droplets).

The diffraction quality of the crystal plates was tested on an in-house imaging detector (MAR Research) coupled to a RU-200 rotating anode X-ray generator (Rigaku) producing Cu Kα radiation with a wavelength of 1.5418 Å.

In the absence of structurally related three-dimensional models, a SeMet-CPO was produced. The purified SeMet-CPO protein was buffer exchanged into 0.07 times PBS pH 7.4, 2 mM DTT or 10 mM MES/NaOH pH 6.5, 2 mM DTT and the best crystallisation conditions obtained for CPO were repeated using microseeding. For this, CPO seeds (prepared as described above) were added to pre-equilibrated droplets containing SeMet-CPO.

6 Results and Discussion

6.1 Tobacco Uroporphyrinogen-III Decarboxylase

The availability of a reasonable amount of protein with a high degree of purity and molecular homogeneity is essential for crystallisation purposes.

SDS-PAGE and N-terminal peptide sequencing assessed the purity and integrity of purified recombinant tobacco UROD. SDS-PAGE showed the presence of a single band corresponding to the molecular weight of the mature protein (39 kDa), and N-terminal peptide sequencing confirmed the correct N-terminal amino acid sequence for the recombinant mature protein (VAEPKA).

6.1.1 Ionic Strength-dependent Dimerisation

Sedimentation equilibrium and Dynamic light scattering (DLS) experiments were performed to verify the oligomerisation and monodispersity of the enzyme.

Sedimentation velocity analysis showed that the protein sediments as a single symmetrical boundary with a velocity of 4.0 S. Sedimentation equilibrium data could be fitted by a single exponential suggesting ideal solute behaviour under the conditions used. The fitted line in Figure 8 was calculated for a mass of 82 kDa. Residuals indicating the close agreement between the theoretical curves and the experimental data are shown in the upper part of the figure. This clearly indicates that tobacco UROD is a homodimer under similar ionic strength conditions to those found in the chloroplast stroma (Neuhaus and Wagner, 2000).

DLS revealed an ionic strength dependence for the protein's oligomeric state. Whereas in the protein buffer (10 mM Tris/HCl pH 7) UROD shows a molecular weight 1.5 times the monomer, the increase of the ionic strength by adding 50 mM of the crystallisation precipitant, ammonium sulphate promotes its dimerisation. Table 2 summarises the DLS results.

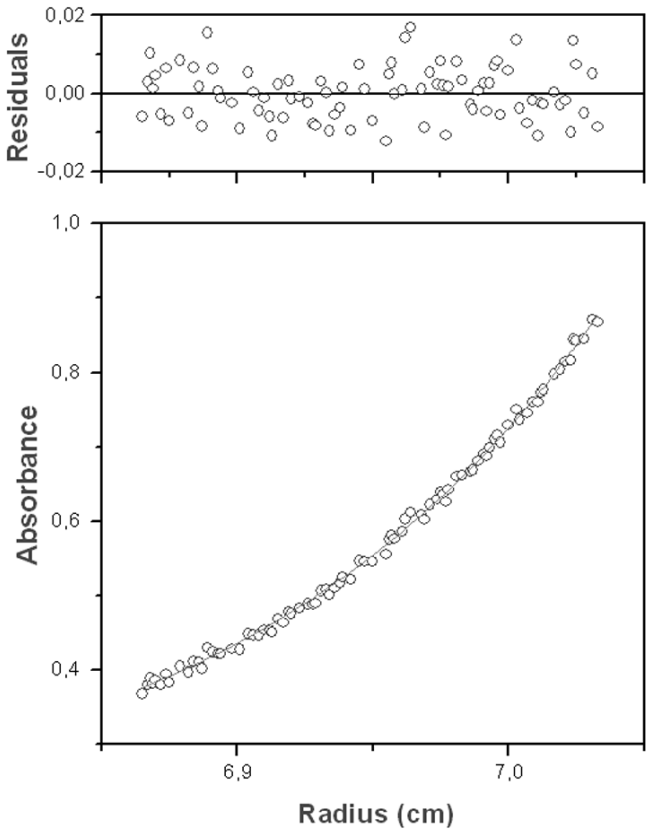

Figure 8 - Equilibrium sedimentation of tobacco UROD. Conditions used were 10000 rpm at 20 °C. Residuals are given on top.

Table 2

Dynamic light scattering data

Protein buffer	Hydrodynamic radius (nm)	Polydispersity index	Estimated MW (kDa)[a]
10 mM Tris/HCl pH 7	3.43	0.07	57.4
10 mM Tris/HCl pH 7, 50 mM $(NH_4)_2SO_4$	3.95	0.1	81.2

[a] Molecular mass was calculated assuming a globular conformation model using the software provided by the manufacturer.

6.1.2 Crystal Growth, Cryoprotection and Data Collection

Based on the calculated isoelectric point of the protein (pI 9.4), the initial crystallisation trials were performed varying the concentration of ammonium sulphate *versus* a

pH range around this pI value. After one to two days a shower of microcrystals appeared in 1.0 M ammonium sulphate pH 10. A further improvement in the crystal nucleation was achieved by varying the precipitant conditions (salt concentration and pH). Thin plates appeared in the presence of several additives but were difficult to reproduce.

Finally, small crystals were obtained in 1.2 M ammonium sulphate at pH 9.6 when the protein was diluted to 2 - 3 mg ml^{-1} and the drop / reservoir ratio doubled. After 18 months the crystals reached dimensions roughly of 400 x 250 x 50 μm^3 (Fig. 9).

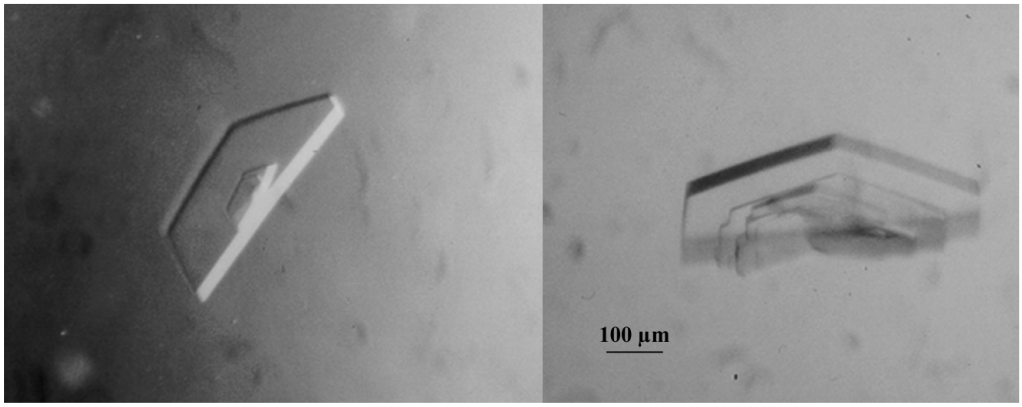

Figure 9 - Crystals of tobacco UROD grown from 1.2 *M* ammonium sulphate pH 9.6 at 20 °C.

In addition to a poor diffraction resolution (3 Å, in house X-ray facility) the crystals were very sensitive to radiation decaying after a few hours of exposition, preventing the collection of complete data sets from single crystals.

The search for a cryoprotectant solution based on the crystal mother solution turned unsuccessful, and only the combination of a new buffer composition together with an increase in the salt concentration made it possible to flash cool the crystals. Ever so, when immersed for more than a few seconds the crystals became yellowish and gelatinous loosing all diffraction power. To overcome this, the crystals had to be rapidly passed through the cryoprotectant solution, which was difficult to reproduce and resulted in the destruction of a large number of crystals. The breakthrough came from pre-equilibrating the cryoprotectant solution in air by 5 - 10 min prior to immersion of crystals. Upon cooling in nitrogen stream (Oxford Cryosystems) the crystals diffracted to 2.3 Å using synchrotron radiation (Fig. 10).

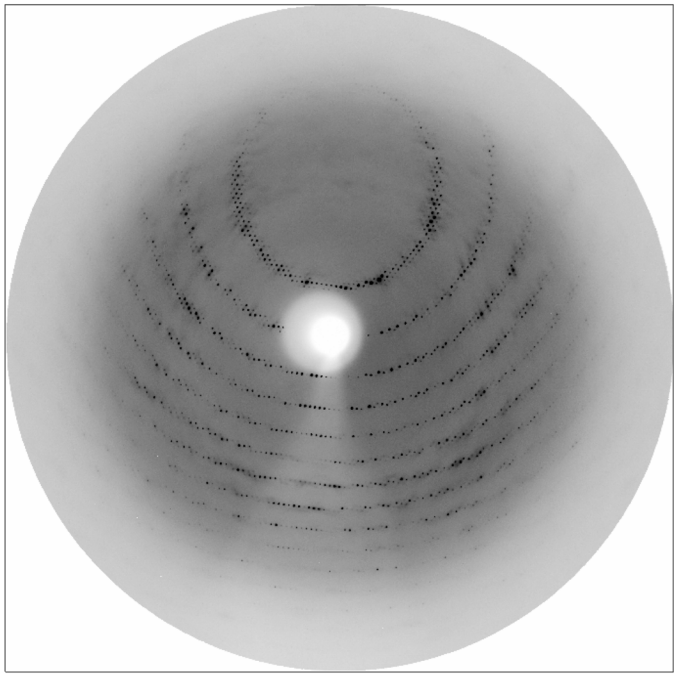

Figure 10 - Diffraction pattern of tobacco UROD crystals. The resolution at the edge of the image is 2.3 Å.

The crystals belong to space group P622 (Fig. 11), with unit cell constants of a = b = 158.44 Å and c = 67.68 Å. There is one molecule per asymmetric unit of the unit cell and the Matthews coefficient of V_m = 3.14 $Å^3$/Da correspond to a solvent content of 61%. This high solvent content may account for the crystal instability when directly exposed to the X-ray beam.

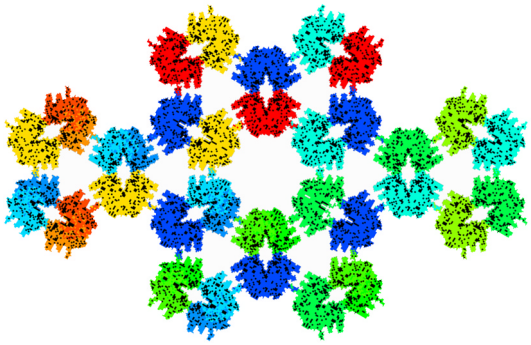

Figure 11 - Crystal's packing of tobacco UROD. The 6-, 3- and 2-fold symmetry axes are readily visible.

A complete data set was collected from a single crystal using a MarCCD detector on wiggler beamline BW6 at DESY (Hamburg, Germany) using synchrotron radiation with a wavelength of 1.05 Å. Data were evaluated using DENZO and SCALEPACK (Otwinowski and Minor, 1996) (statistics are depicted in Table 3).

Co-crystallisation experiments only reproduced crystals in the presence of uroporphyrin-III. Albeit displaying a similar habit, the crystal nucleation seemed to be slower (~2 –3 months for the first optical detection). Additionally, the crystals stop growing after reaching dimensions of roughly 100 x 100 x 20 μm^3. This may account for the weak diffraction power (8 - 6 Å) when tested in an imaging plate detector under cryoprotectant conditions.

All attempts to soak crystals with inhibitors resulted in their destruction immediately after few minutes of soaking. Within the asymmetric unit, the tobacco UROD molecule makes crystal contacts with three symmetry-related molecules. The largest protein-protein interaction is the crystallographic dimer interface that covers more than 1380 Å of solvent accessible surface area per monomer. Two other crystal contacts involve only thirteen and one residue, respectively. Thus the molecule's active site cleft is neither facing the 6- nor the 3-fold axis, which together with the relative large dimensions of the inhibitor molecules, may explain the impossibility to obtain soaked crystals due to their lattice destruction.

6.1.3 Patterson Search and Model Refinement

The three-dimensional structure of tobacco UROD was solved by molecular replacement using the human homologous protein (PBD accession code 1URO). The search model consisted of a truncated protein with residues Gly10 - Thr31, Ala251-Pro257 and Ile341 - Asn366 removed and non-conserved residues replaced by alanine. The best solution calculated with the program AMoRe (Navaza, 1994) had a correlation of 38.1 % and an R-factor of 51.3 % (the values for the second best one were 27.6 % and 51.4 %, respectively) in the resolution range between 15 and 4 Å.

Model refinement was performed by iterative rounds of building in MAIN (Turk, 1992) and refinement using CNS (Brünger *et al.*, 1998). The refined model has a R_{cryst}-factor of 20.94 % (R_{free}-factor of 25.57 %) and good stereochemistry (refinement statistics in Table 3).

The final model comprises the amino acid residues Thr10 - Tyr352, 250 water molecules and 5 sulphate ions. The complete polypeptide chain could be traced with the exception of the first nine amino acid residues. Residues Gln33 – Leu60 were fixed through the refinement steps due to their discontinuous ($2F_{obs}$ - F_{cal}) electron density map, and poorly defined side chain for residues at the protein's surface were modelled with half occupancy. One solvent molecule and two sulphate ions, located at two-fold symmetry axis were modelled with half occupancy and fixed during the refinement cycles.

Table 3

Data collection, refinement and model quality statistics

PARAMETER	UROD
Data collection	
Resolution range (last shell) (Å)	18.00 - 2.30 (2.34 - 2.30)
Reflections (collected / unique)	47385 / 22173
Completeness (last shell) (%)	97.7 (98.3)
R_{sym} (last shell) (%)[a]	6.0 (34.6)
I/σ(I) (last shell)	26.1 (4.3)
Model refinement	
Resolution range (Å)	18.00 - 2.30
No. of reflections (2σ cutoff)	21792
R_{crys}-factor (%)[b] / R_{free}-factor (%)[c]	20.94 / 25.57
Average B-factor for protein (water) (Å^2)	39.27 (47.70)
r.m.s.d. for bonded B-factors (Å^2)	1.507
r.m.s.d. in bond lengths (Å)	0.007
r.m.s.d. in bond angles (°)	1.225
Ramachandran outliers[d]	none

[a] $R_{sym}=\sum|I-<I>|/\sum(I)$, where <I> is the average intensity for multiple observations of symmetry related reflections.

[b] $R_{cryst}=\sum||F_{obs}|-|F_{cal}||/\sum F_{obs}$, where F_{obs} and F_{cal} are observed and calculated structure factors amplitudes, respectively.

[c] R_{free} is the cross-validation R-factor computed for the test set of reflections (5 % of total number of reflections) randomly selected and not included in the refinement.

[d] Program PROCHECK (Laskowski *et al.*, 1993).

6.1.4 Structural Analysis: Implications for the Catalytic Mechanism

6.1.4.1 Overall Topology

The tobacco UROD molecule comprises a single domain with approximate dimensions of 58 x 40 x 43 $Å^3$. The protein displays a broken $(\beta\alpha)_8$-barrel fold with seven parallel β-strands forming a circular β-barrel that is surrounded by seven α-helices and one 3_{10}-helix linking the seven neighbouring β-strands (Fig. 12). Residues Pro27 - Trp29, approximating β-conformation and the helix 3_{10}-III would allow the closure of a complete $(\beta\alpha)_8$-barrel motif.

The amino acid composition of a $(\beta\alpha)_8$-barrel protein has an essential role in the formation of its β-barrel core which could be particularly disrupted by proline residues (Nagano *et al.*, 1999). The presence of Pro26 preceding residues Pro27 - Trp29 explains the disruption of the β-barrel by impairing their β-strand conformation.

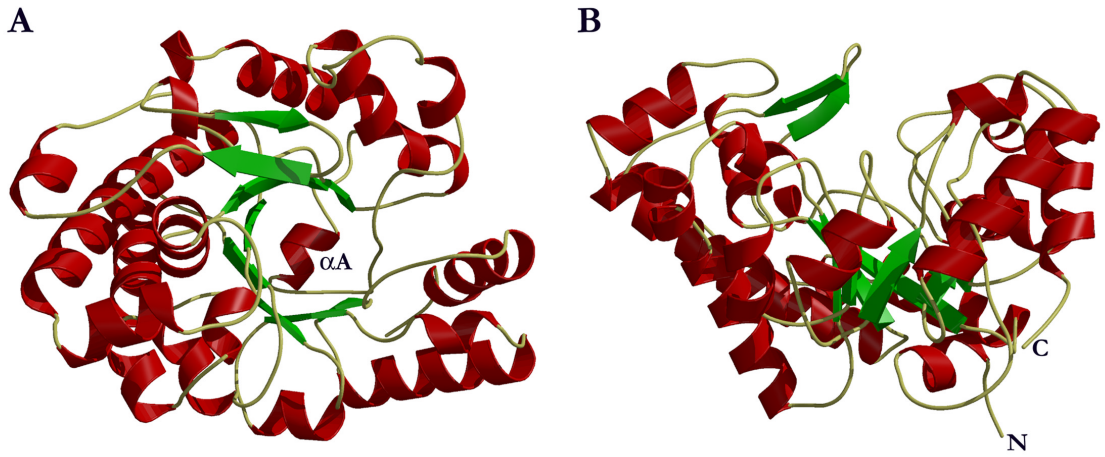

Figure 12 - **Overall structure of tobacco UROD**. For simplicity helices are depicted in red and β-strands in green. ***A***, front view of the molecule: at the bottom, αA closes the N-terminal end of the β-barrel core and several loops surround the C-terminal end at the top. ***B***, side view: the C-terminal loops are easily seen above the β-barrel core. The protein N and C termini are labelled. For a more detailed discrimination of the secondary structure elements extra to the $(\beta\alpha)_7$-barrel see Fig. 14 A.

Particular sets of residues lying perpendicular to the β-barrel axis pack in two to five layers building its core (Nagano *et al.*, 1999). In tobacco UROD, four stacked layers build up the β-barrel core with a diameter of approximately 15 Å (distance between the amino acids Cα) and almost circular cross-section (Fig. 13).

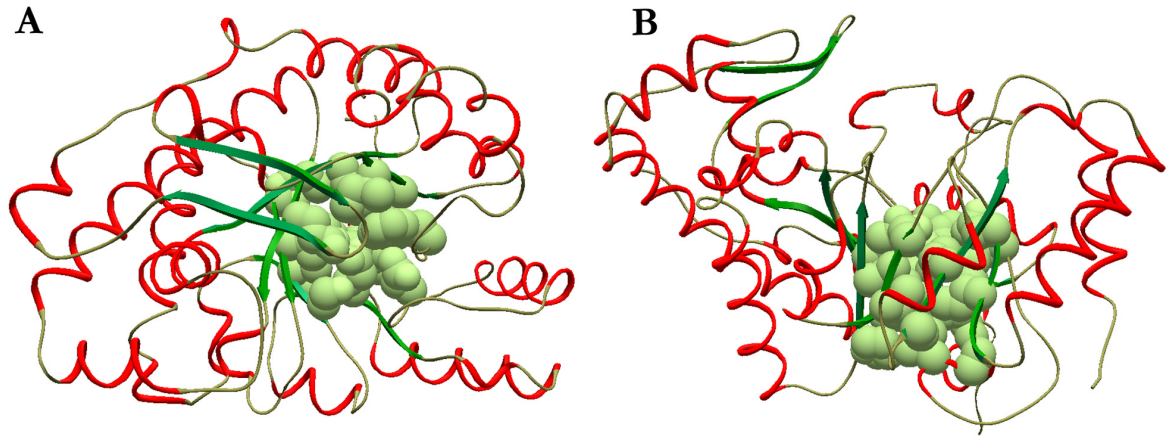

Figure 13 - **The β-barrel core from tobacco UROD.** The residues involved in the core are represented by their Van der Waals surface (same orientation as in Fig. 12).

The $(\beta\alpha)_7$-barrel comprises β-strands β1 and β4 to β9, and α-helices αC, αE and αH to αM (Fig. 14 A). All the helix-strand turns at the N-terminal end of the β-barrel are constituted by only a few residues, while larger segments can be observed at its C-terminal end. Thus, compared to a "minimal" $(\beta\alpha)_8$-barrel architecture, tobacco UROD contains additional secondary structural elements restricting the access to the interior of the β-barrel. The N-terminal end is capped by helix αA, anchored to the protein through hydrophobic interactions with the β-barrel layers, while several extended loops surround the wider C-terminal end. The additional secondary structure elements may play an extra role in intermolecular interactions within the hypothetical physiologic dimer, discussed below.

The sequence of UROD has been considerably conserved throughout evolution with overall 33 % similarity (Mock *et al.*, 1995) with two unique signature patterns (Prosite documentation access number PDOC00705) (Garey *et al.*, 1992). The highest homologous one, located near the N-terminus contains a perfectly conserved hexa-peptide (Pro27 - Arg36 in tobacco UROD), while the second is based on a well-conserved region located in the central part of the protein (Gly148 - Gly163 in tobacco UROD).

The amino acid sequence alignment for UROD from tobacco (plant), human (mammal), *E. coli* (bacterium) and *A. eolicus* (archea), together with the location of the secondary structure elements for the tobacco model is depicted in Fig. 14 B.

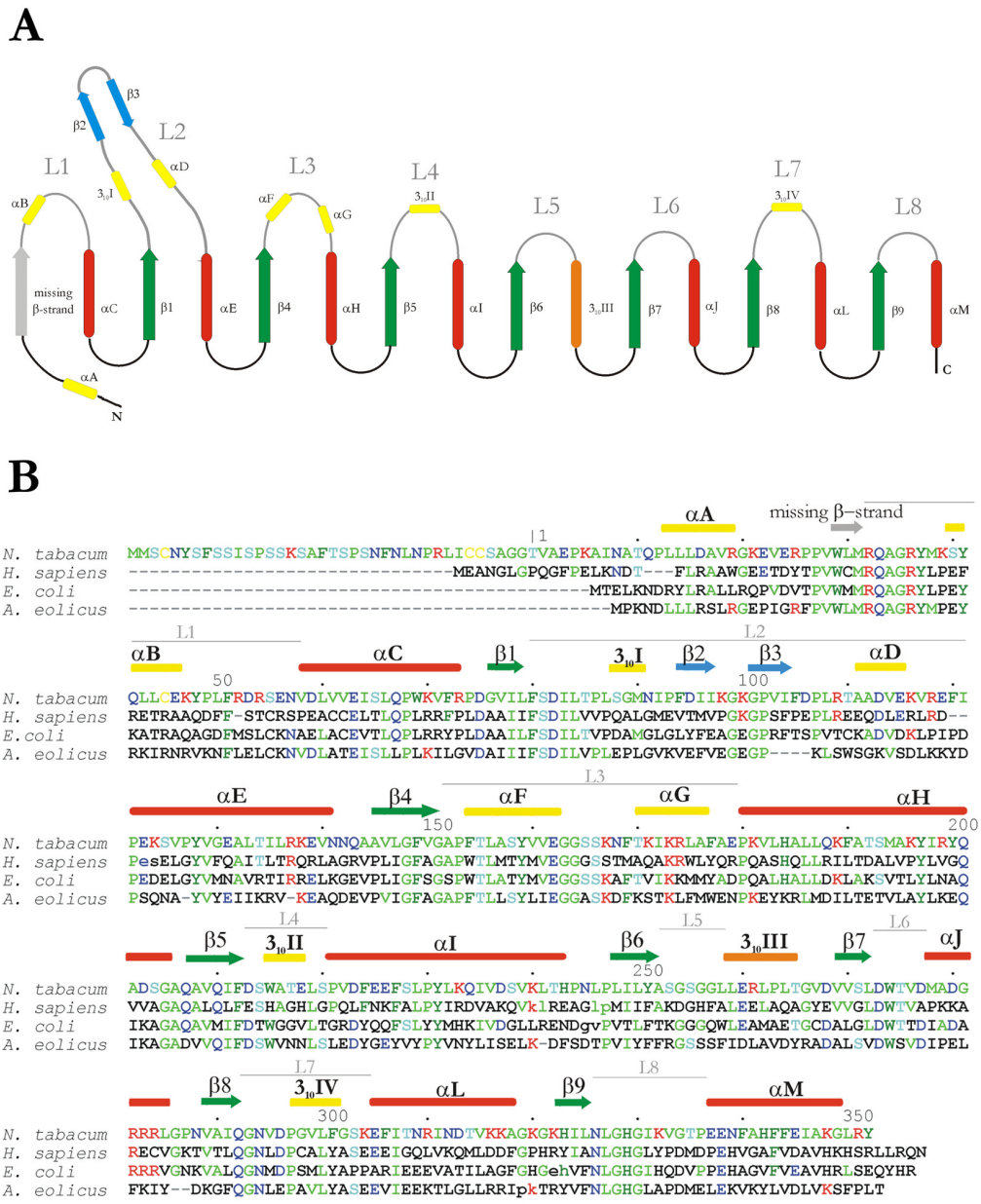

Figure 14 - A: Topology diagram of tobacco UROD. The α-helices and β-strands forming the β-barrel core are colored in red and green, respectively and loops L1 to L8 are marked by a grey line. Helix 3_{10}III is colored in orange and the missing β-strand in gray. Helices and β-strands extra to the β-barrel are depicted in yellow and blue, respectively. For respective peptide sequence see B. **B: Sequence alignment** for tobacco, human, *E. coli* and *A. eolicus* URODs. The residue numbering refers to the mature tobacco sequence. The bar | indicates the cleavage site of the N-terminal plastid targeting

sequence of tobacco UROD. Small letters indicate amino acid insertions relative to the tobacco sequence. *N. tabacum*: *Nicotiana tabacum* (Q42967); *H. sapiens*: *Homo sapiens* (Q16883); *E. coli*: *Escherichia coli* (P29680); *A. aeolicus*: *Aquifex aeolicus* (O66667).

6.1.4.2 Dimeric Form

Tobacco UROD was crystallised in space group P622 with one molecule per asymmetric unit of the crystal unit cell. Using a 2-fold crystallographic symmetry axis, this monomer forms a dimer similar to the homologous human enzyme (Whitby *et al.*, 1998). Superposition of tobacco and human dimers has a root mean square displacement of 1.67 Å for all Cα atoms. This value is higher than the calculated one for the individual monomers' superimposition (1.12 Å) (Fig. 15 B) and can be explained by a slightly different arrangement of the protein subunits in the dimers.

The dimer displays a head-to-head arrangement with overall dimensions of approximately 70 x 40 x 43 $Å^3$ (Fig. 15 A).

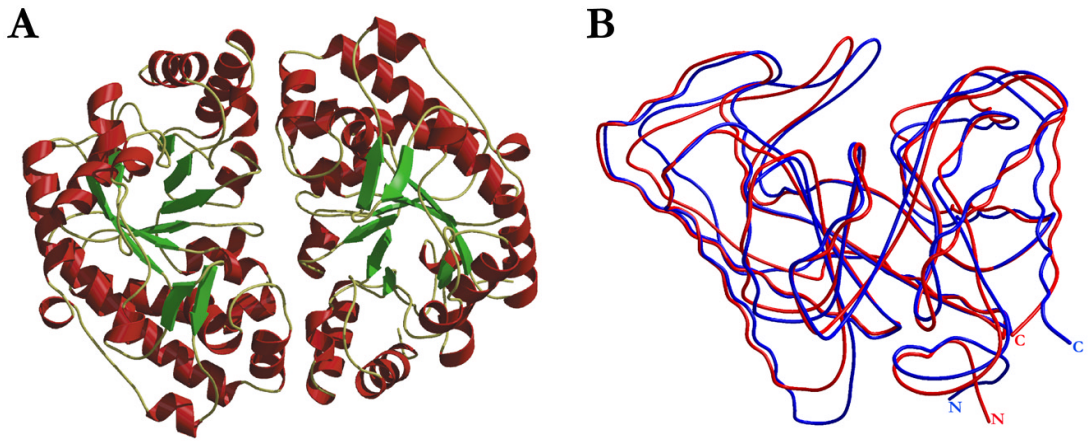

Figure 15 - A, The crystallographic dimer of tobacco UROD. The dimer displays a head-to-head arrangement due to the unit cell two-fold symmetry axis (perpendicular to the plane of the figure) with the extensive flat dimer interface burying more than 1380 $Å^2$ ASA per monomer. Colour code as for Figure 12. **B, superposition of Cα atoms from tobacco and human URODs**. Colour code: red and blue for the tobacco and human proteins, respectively. The respective N and C termini are labelled.

The flat dimer interface is extensive and largely hydrophilic involving 11 direct hydrogen bonds and salt bridges. Part of these interactions involve residues from secondary

structure elements extra to the $(\beta\alpha)_7$-barrel motif, namely helices αG, 3_{10}-II and 3_{10}-IV. In addition, 19 of the 30 solvent molecules buried upon dimerisation form hydrogen bonds with residues in both monomers, thus contributing to the hydrogen-bonding network at the dimer interface. Solvent mediated polar interactions are more numerous than direct hydrogen bonds with one interface water per 92 Å^2 ASA compared to one direct hydrogen bond per 250 Å^2 ASA. These values are in good agreement with results obtained from structural analysis on protein-protein interaction (Conte *et al.*, 1999).

Although protein crystal contacts are tenuous and generally form only under conditions designed to limit protein solubility and maximise protein-protein interactions, the oligomeric state observed in crystals can reflect a biological function (Dasgupta *et al.*, 1997). In tobacco UROD, more than 1380 Å^2 per monomer's solvent accessible surface area (ASA) are buried at the dimer interface. This value is well above the ASA mean value of 280 Å^2 per monomer, typical for random packing interactions in protein crystals (Janin and Rodier, 1995).

Equilibrium sedimentation and dynamic light scattering analysis with the protein sample producing diffracting crystals clearly shows a dimeric state for tobacco UROD in solution (see section 5.1.1). As a similar dimer has been observed in the human UROD crystal structure, it is presumed to display the protein dimer under physiologic conditions.

6.1.4.3 The Catalytic Cleft

In common with other $(\beta\alpha)_8$-barrel proteins, different regions of the tobacco UROD sequence contribute with residues to the catalytic cleft located at the C-terminal end of the β-barrel core. The extended loops L1, L2, L3 and L4 together with loops L5, L6 and L8 build up an funnel-like cleft with approximated dimensions of 14 x 12 x 12 Å^3 (Fig. 16 A). The β-hairpin in loop L2 forms a *lid* partially covering its top entrance.

6.1.4.3.1 The Funnel Architecture

A striking feature of the *funnel* is its incomplete enclosure. Whereas the *funnel* spans from bottom to top of the cleft accounting for most of its walls, the short loops L5, L6 and L8 contribute with residues mainly to the bottom part, thus leaving the top edge of the *funnel* exposed to solvent. This structural feature is difficult to conceive with shielding the substrate

from solvent contact inside a closed catalytic cleft, but might be essential for catalysis. Interestingly, the same exposed flanking region is involved in the dimer interface. The mechanistic implications from this structural feature will be discussed later.

Several strictly and well-conserved side chains line the walls of the catalytic cleft. For a simple enumeration they were grouped into three regions, base, bottom and top edge. The top stacked layer of the β-barrel core forms the base of the cleft. Residues Phe149, Phe212, Ser214 and His329 build the bottom part, while Arg32, Arg36, Tyr41, Phe80, Asp82, Tyr159 and Trp215 line the top edge (Fig. 16 B). A superimposition of the catalytic clefts from tobacco and human URODs shows the general structural conservation of these side chains (Fig. 16 C). Three other polar side chains strictly conserved among the known plant URODs are positioned at the top edge, namely Arg54, Ser55 and Ser253.

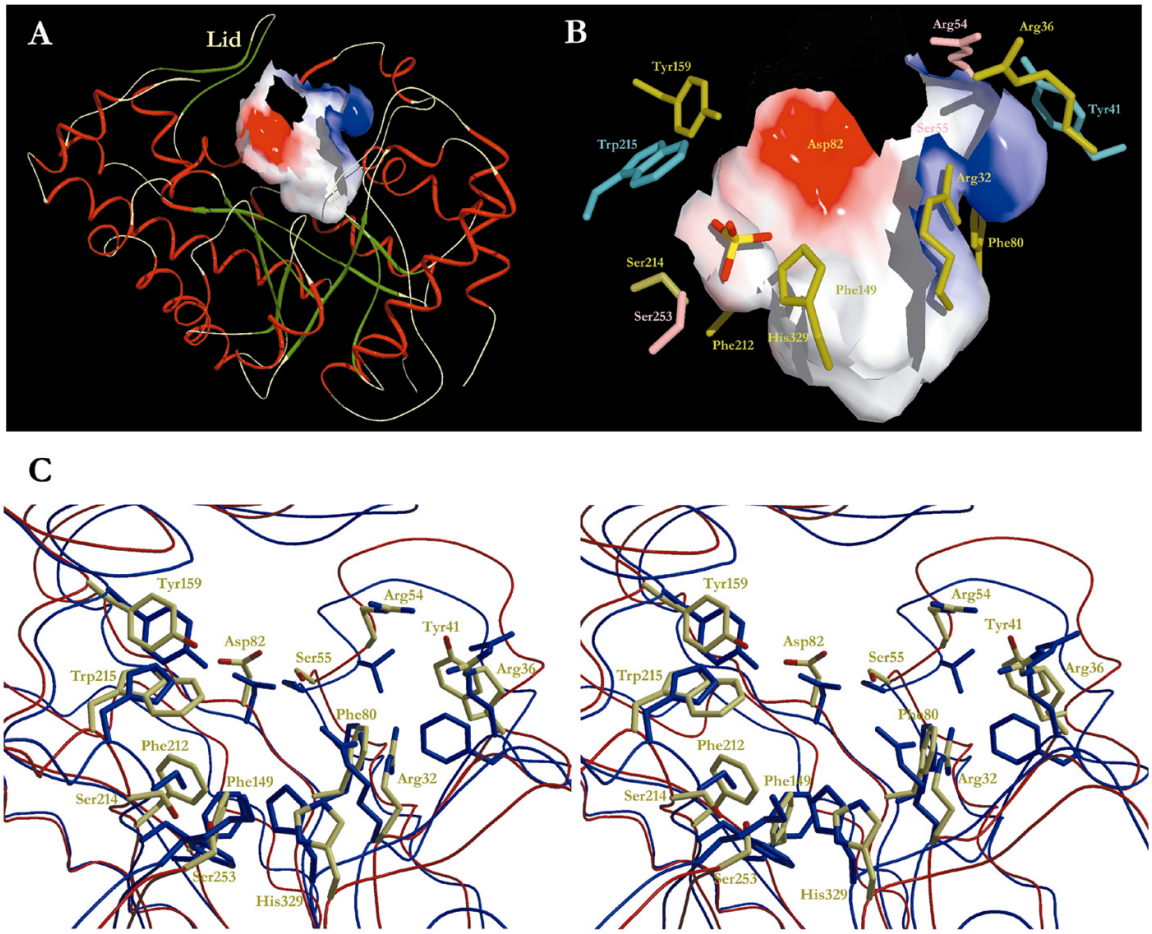

Figure 16 - The catalytic cleft of tobacco UROD. A: front view. The loops from the *funnel* wrap the back and left (reader view) surface of the cleft. Loops L5, L6 and L8 surround the bottom (reader view) side of the cleft. Loop L7 at the right front side (reader view) of the *funnel* doesn't contribute with residues to its formation. **B**: close view. Invariant residues are coloured in olive green and well-

conserved ones in cyan. Ser214 is coloured in olive green since it is strictly conserved in all know sequences except for *E. coli*. Residues strictly conserved among plants are coloured in salmon. In this orientation Ser55 and Asp82 are at the back of the cleft's surface and Phe149 behind His329. The sulphate ion in coloured according to atom type (yellow for sulphur and red for oxygen). **C**: stereo view of the superimposed clefts from tobacco and human URODs. For simplicity only the tobacco residues are labelled. Colour code for tobacco UROD: red for Cα trace, olive green for carbon, blue for nitrogen and red for oxygen atoms; for human UROD: blue for Cα trace and side chains.

Analysis of x-ray crystallographic data from protein-ligand complexes including enzymes from the tetrapyrrole metabolism (Louie *et al*., 1992) (Frankenberg *et al*., 1999) indicates that carboxylate groups not removed during catalysis are usually stabilised through salt bridges with positively charged residues. Consistently, in addition to Arg32, Arg36 and His329, we find several other positive side chains wrapping the top edge, namely Lys39, Lys47, Arg54, Lys98, Lys100 and Lys167.

In contrast to the positively charged flanking regions, the cleft's surface is hydrophobic with exception for two polar patches, and displays one protrusion and two grooves (Fig. 16 B). Asp82, responsible for one of those polar patches sticks out of the surface producing the protrusion. The second patch coincides with the positively charged groove in the top edge formed by Arg32, Arg36 and Arg54. Residues Phe212, Ser214, Trp215, Ser253 and His329 line the groove in the bottom part. Inside this groove, additional clear electron density was observed and modelled as a sulphate ion, with all the oxygen atoms involved in a dense hydrogen bond network with those residues.

6.1.4.3.2 Tracing the Catalytic Residues

The catalytic mechanism of UROD has been studied in great detail. One important result is that in the conversion of uro-III into copro-III the acetate side chains of rings D, A, B and C are decarboxylated in a clockwise fashion starting at ring D (Jackson *et al*., 1976a). Other fundamental aspects were revealed by stereochemical studies (Barnard and Akhtar, 1975, 1979). The two methylene hydrogen atoms of the acetate side chain remain undisturbed and a new C-H bond replaces the carboxylate group with retention of configuration. Based on these results a mechanism was proposed involving protonation of one α-position of the pyrrole ring moiety. This tautomerisation promotes electron withdrawal from the acetate side chain

resulting in CO_2 liberation. At physiological pH uro-III will be ionised and may be linked to a conjugate acid by a hydrogen bond.

All of the 24 possible decarboxylation reaction sequences for uro-III can generate the reaction product, copro-III. However, UROD sequentially removes the carboxylate groups starting at ring D, indicating specific protein-ligand interactions within the catalytic cleft. It is believed that certain residues in close proximity function both in the decarboxylation of the acetate side chain and the stabilisation of the neighbouring propionate side chain. In addition, in close proximity to these residues a recognition site for the pyrrole nitrogens is required (Akhtar, 1994). No specific catalytic acid/base group has been proposed to perform the protonation of the pyrrole ring moiety.

Apart from Arg32 and Arg36, the only other invariant polar residues present within the cleft are Asp82, Tyr159 and His329, being therefore the prime candidate residues for catalysis.

The presence of a patch of a negative charge (Asp82) in the cleft's hydrophobic environment is conspicuous. Under physiological conditions aspartate residues are usually ionised but an apolar surround can greatly increase their pKa values. Thus, when protonated Asp82 would be the ideal residue to involve the acetate side chains of the substrate in a hydrogen-bonded structure, and to protonate the intermediate methylene side chain. Tyr159 is located in close proximity to Asp82 and its side chain is relatively exposed within the cleft making it a candidate for the protonation of one α-position in the pyrrole ring moieties. The third invariant residue is His329, located opposite to Asp82 and Tyr159. The nearby groove buries a sulphate ion indicating a possible anchoring site for the substrate side chains. This residue was shown not to be essential for catalysis, being most likely involved in isomer recognition and alignment of reaction intermediates within the catalytic cleft (Wyckoff *et al.*, 1996), (Whitby *et al.*, 1998).

Inside the catalytic cleft, Phe80 (Tyr in *B. subtilis*), Phe149 and Phe212 can stack against the pyrrole ring moieties as observed for other enzymes from the same metabolic pathway (Frankenberg *et al.*, 1999) (Louie *et al.*, 1992).

6.1.4.4 Modelling of Enzyme-Substrate Complexes for Human and Tobacco

Without structural information from crystals of tobacco and human UROD associated with substrate, product, inhibitor or analogues of substrate or product, enzyme substrate complexes were modelled using the program package InsightII.

The uro-III molecule is flexible due to a non-fully conjugated ring system. Therefore it appeared useful to perform the modelling calculations with an experimentally determined uro-III structure. Unfortunately, the screening of all known available chemical and structural databases resulted in only one crystal structure for a homologous compound, uroporphyrinogen-octanitrile (type-I) tetrahydrofuran solvate (Cambridge Structural Database, http://www.ccdc.cam.ac.uk/prods/csd/) (Lehmann *et al.*, 1997). This compound was modified in module Builder (InsightII) into an uro-III molecule by changing the nitrile groups into carboxylate groups retaining the orientation and taking into account the asymmetric distribution of the acetate and propionate side chains in ring D. The modelling of the enzyme substrate complex was started with human UROD.

6.1.4.4.1 Human Enzyme-Substrate Complex

In the 1.6 Å resolution crystal structure (Whitby *et al.*, 1998) only the amino acid stretch Met100-Gly105 lying on top of the catalytic cleft is poorly defined. All other parts of the catalytic cleft including side chains are well defined. Asp86, located in a hydrophobic environment (Phe46, Phe55, Phe84, Ile87 and Phe154) appears to be the conjugate acid postulated in the proposed catalytic mechanism (Barnard and Akhtar, 1975). Tyr164 seems to be a good candidate for the protonation of the pyrrole ring α-position. Taking into account these assumptions the uro-III molecule was manually positioned in such a way that the acetate groups of rings D and A were directed against the carboxyl group of Asp86 and the hydroxyl group of Tyr164, respectively (Fig. 17 A). Asp86 was protonated to allow a hydrogen bond interaction with the acetate group of ring D. The tetrapyrrole ring system was positioned above the side chain of Arg37. In this modelling it is postulated that Arg37 functions as guiding group to the highly negatively charged substrate into the catalytic cleft.

The energy minimisation with module Discover3 finished after 1000 steps with an energy value of 1174 kcal / mol and the resulting model is depicted in Fig. 17 B. There are polar contacts to the side chains of all invariant residues except of Arg37, the steering group. The propionate side chain of ring D is in a peculiar hydrophobic environment, which may stabilise it. Tyr164, nearby localised could perform the protonation of one α-position at this pyrrole ring moiety.

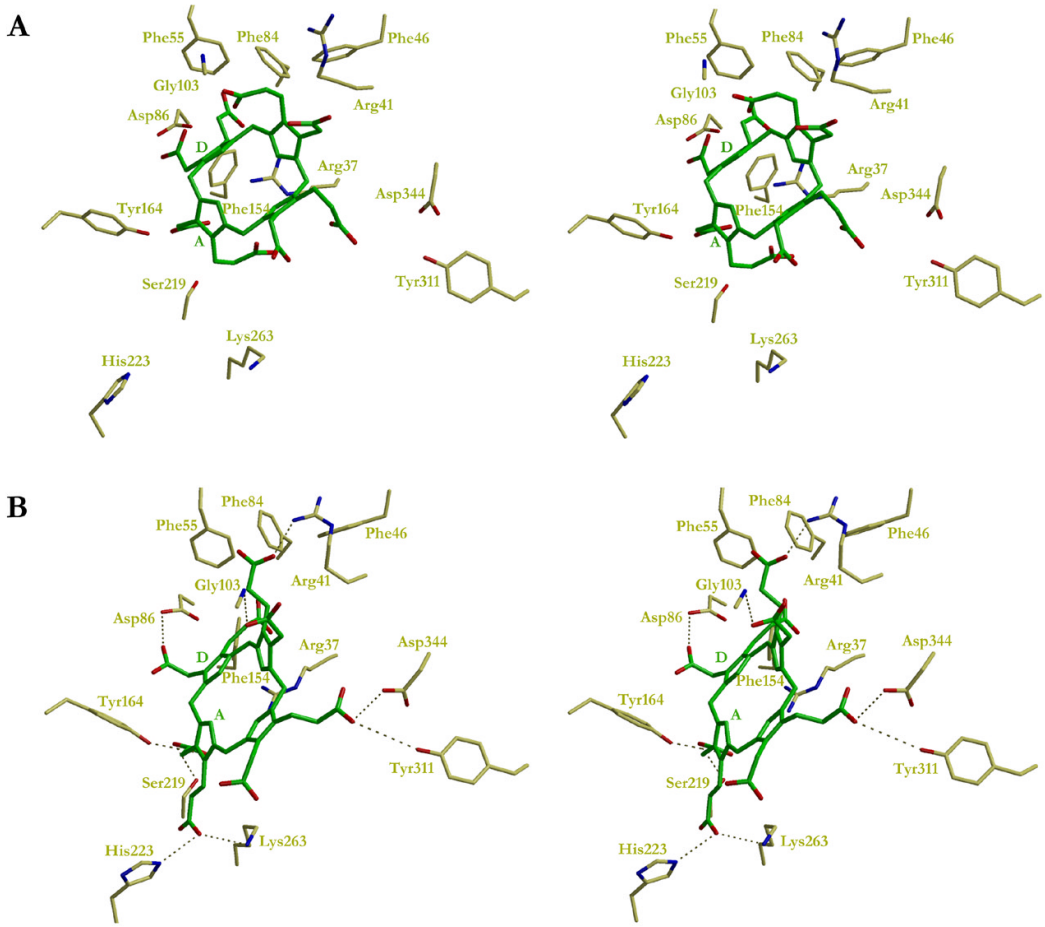

Figure 17 - Modelled enzyme substrate complex for human UROD. **A**: the initial substrate enzyme complex. **B**: the complex after energy minimisation. Dash lines represent putative electrostatic interactions between the substrate and the enzyme. The substrate is depicted in green with exception for the oxygen atoms (in red). Protein residues are coloured according to atom type, olive green for carbon, blue for nitrogen and red for oxygen. Labelled residues are numbered according to the human amino acid sequence (Whitby *et al.*, 1998). For simplicity only rings A and D from the substrate are labelled.

6.1.4.4.2 Tobacco Enzyme-Substrate Complex

The modelling for the enzyme substrate complex of tobacco UROD was performed in a similar way as for human UROD. Here one has to notice that the amino acid stretch Gln33-Leu60 which holds the polar residues Arg36, Arg54 and Ser55 is only poorly defined in the electron density and therefore more flexible. The initial substrate molecule with the same conformation as in the human UROD calculations, was manually positioned in such a way that both acetate groups of rings D and A were in hydrogen bonding distance to the carboxylic group of Asp82 and the hydroxyl group of Tyr159, respectively. The tetrapyrrole

ring system was placed on top of the side chain of Arg32, the steering group for substrate insertion in tobacco UROD. In order to have a structural arrangement of the catalytic cleft similar to the human homologous protein, this side chain was placed in the same orientation as the corresponding residue in the human model (Fig. 18 A).

The differences of the active sites of both enzymes have been already described above. However, the most important substitutions for protein-substrate interaction are the presence of Trp215 (His220 in human) and Arg54 (Thr58 in human). In tobacco UROD, Trp215 has a larger side chain making the binding pocket tighter at this region, and the side chain of Arg54 is in the vicinity of the propionate side chains of rings D and C.

The result of the energy minimisation is depicted in Fig. 18 B. Albeit proportioning a higher number of polar contacts, the narrower binding pocket in the tobacco enzyme results in a more stressed substrate enzyme complex (reflected in a higher total value for the energy minimisation, 2713 kcal / mol).

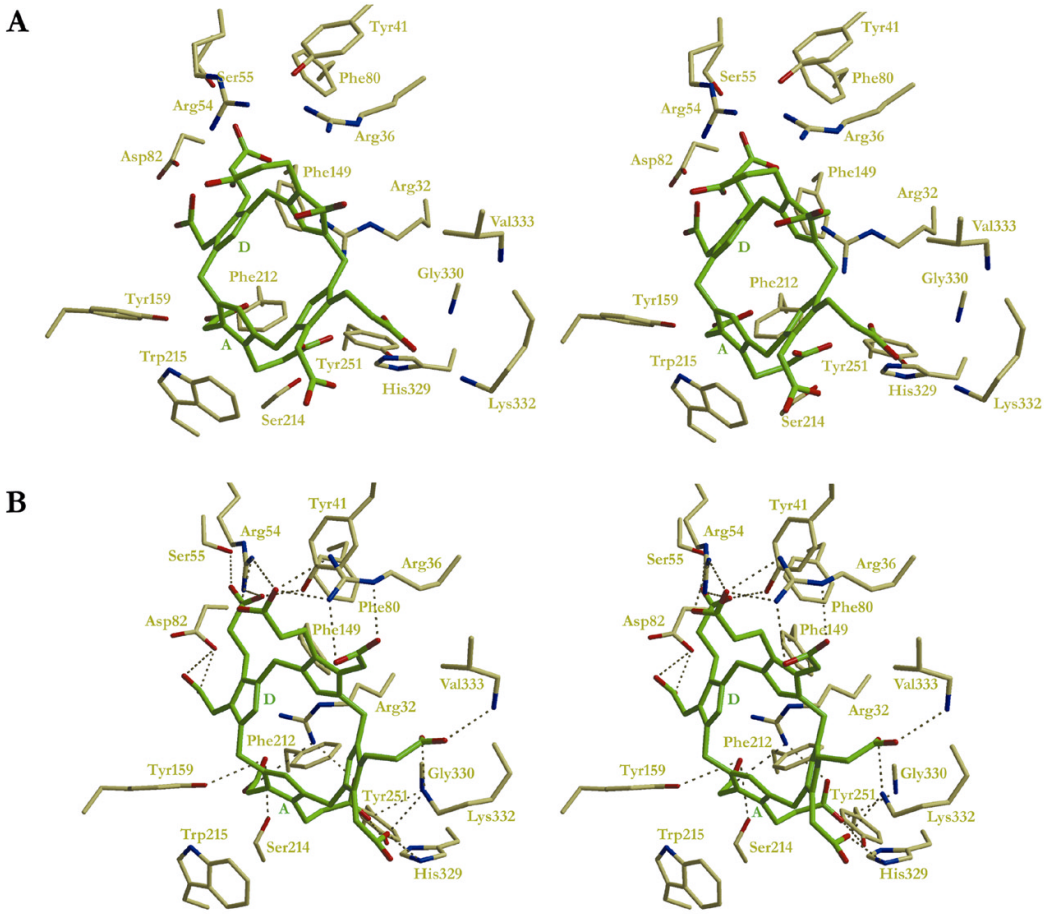

Figure 18 - Modelled enzyme substrate complex for tobacco UROD. A: the initial substrate enzyme complex. **B**: the complex after the energy minimisation. Dash lines represent the putative electrostatic

interactions between the substrate and the enzyme. Colour code is the same as for figure 17. Labelled residues are numbered according to the tobacco amino acid sequence (see Fig. 16 C). For simplicity only rings A and D from the substrate are labelled.

6.1.4.5 Proposal for a Refined Catalytic Mechanism

The careful inspection of the two UROD crystal structures and the results of the enzyme substrate modelling calculations supports a modified catalytic reaction scheme based on a previous suggestion (Akhtar, 1994), and is depicted in Fig. 19.

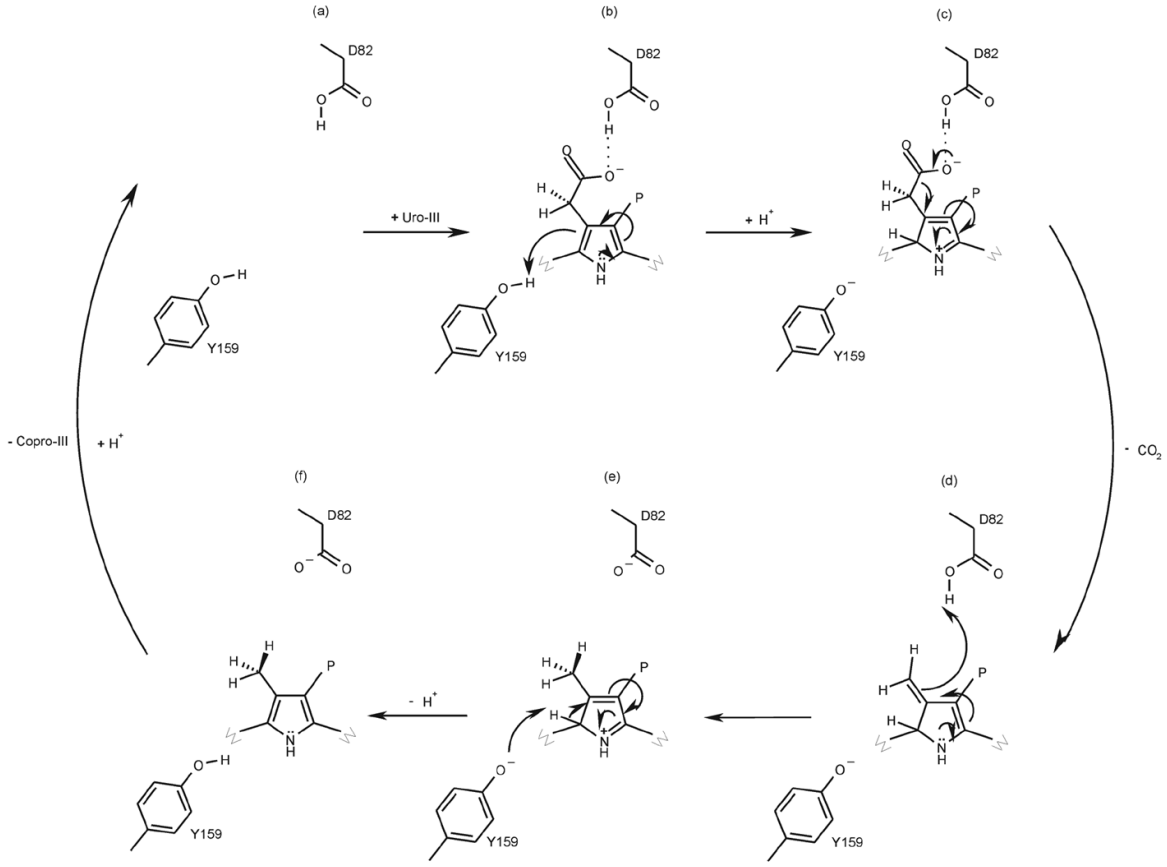

Figure 19 - Putative reaction sequence for the UROD catalysis. For simplicity only one pyrrole ring moiety is depicted. The sequential steps, (a) to (f) are explained in the text.

We start with the free enzyme (Fig. 19 (a)) where both Asp82 and Tyr159 are protonated. The first step is the binding of the uro-III molecule to the catalytic cleft with the acetate side chain of ring D at hydrogen bond distance to Asp82 (Fig. 19 (b)). Due to its high π-electron density the α-position may be protonated by Tyr159, generating a tautomeric form of the pyrrole ring (Fig. 19 (c)). Electronic rearrangements weaken the bond of the carboxylate

group leading to the release of CO_2 and the formation of an intermediate methylene side chain (Fig. 19 (c), (d)). Next, the methylene group is protonated by Asp82 yielding the final methyl group (Fig. 19 (e)), and the tyrosinate anion (Tyr159) abstracts the proton from the pyrrole α-position restoring the initial tautomeric form of the pyrrole ring (Fig. 19 (f)). The decarboxylated product leaves the catalytic cleft, Asp82 is protonated by a solvent molecule present in the substrate-free protein, and the enzyme returns to its initial state (Fig. 19 (a)).

6.1.4.6 Dimer-dependent Catalysis?

In the dimer, the two active site aspartates 82 are 35 Å apart and the catalytic clefts are partially restricted by loop L3 from the other monomer (Fig. 20 A, B). A large number of residues involved in the dimer interface are relatively well conserved in all known UROD sequences, suggesting that the dimer formation is a common property of this protein family.

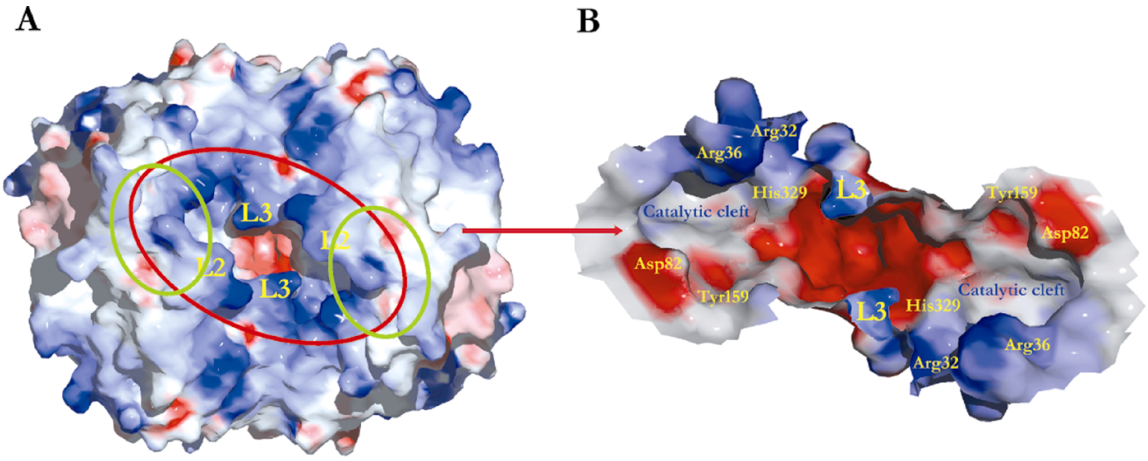

Figure 20 - The spatial arrangement of the two catalytic clefts within the UROD dimer. A: molecular surface representation of the electrostatic potential of the dimer (same orientation as in Fig. 15). Negatively charged residues are represented in red and positively charged ones in blue. The top narrow opening is roughly 14 x 12 $Å^2$ (surrounded by the red circle) and is located directly above the dimer interface. The two green circles indicate the orientation of the two monomeric catalytic clefts. **B**: by removing loops L2 it is possible to observe the wide hole connecting the unprotected bottom part of both catalytic clefts.

The sequential decarboxylation of uro-III requires that, in order to bring the side chains of ring A to the positions previously occupied by the ones of ring D the first reaction

intermediate must flip 180 ° around its C_{10}-C_{20} axis (see Fig. 5) (Jackson *et al.*, 1976b), (Luo and Lim, 1993). The restricted volume (14 x 12 x 12 □^{3}) of the catalytic cleft turns this spatial rearrangement difficult to fulfill, if not impossible. The dimeric form offers a plausible model for this second decarboxylation to occur without the flipping rearrangement.

Modelling studies of substrate binding by the dimer showed that the access of substrate to any of the catalytic clefts is partially hindered by loop L3. After the initial decarboxylation at ring D, the first intermediate can move over the ridge formed by the polar residue at the tip of loop L3 (Lys, Arg or Ser) (Fig. 20 B) into the second monomer. Consistent with this, we find a concentration of positive side chains in the regions flanking the dimer opening that may guide this transfer (Fig. 20 A).

Since the last two decarboxylation steps require each only a 90 ° rotation around the axis perpendicular to the ring system, they may take place in this second catalytic cleft. Thus the dimer can efficiently trap the reaction intermediates in the cleft's vicinity during catalysis. Additionally, this would diminish the risk of loosing the photoreactive metabolites into the cellular medium, which can cause severe cell damages including the onset of apoptosis.

Regions of the protein surface forming extensive crystal contacts are candidates for specific interactions with partner molecules, mimicking functional interactions of the protein in its natural environment (Janin and Rodier, 1995). The dimer interface can have an extra functional role in heteroligomerisation, thus providing a first insight into the putative substrate channelling in tetrapyrrole biosynthesis.

6.2 *E. coli* Oxygen-dependent Coproporphyrinogen-III Oxidase

6.2.1 High Yield One-Step Purification

Recombinant *E. coli* oxygen-dependent coproporphyrinogen-III oxidase was over-expressed in BL21 (DE3) cells up to 20 mg of pure protein per culture litre.

N- and C-termini sequence were verified by peptide sequencing. The purified protein appeared as a single band of molecular mass around 35 kDa on SDS-PAGE kDa (Fig. 21), which is in good agreement with the value obtained from ES-MS (35390 Da) and the predicted his-tagged protein (35387 Da, ProtParam tool, Expasy, http://www.expasy.org/tools/protparam.html).

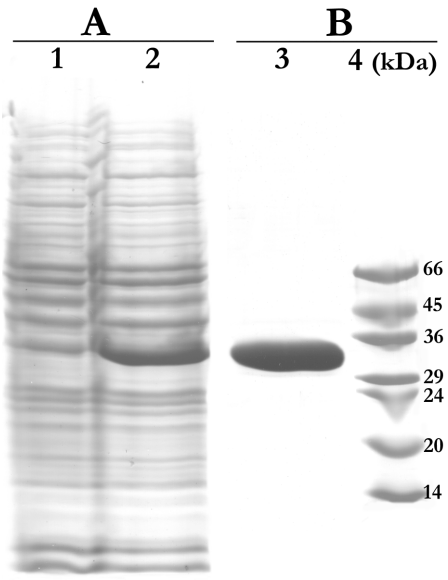

Figure 21 - Homologous over-expression and purification of *E. coli* CPO (12 % SDS-PAGE). A: cell lysates from non-induced (lane 1) and induced (lane 2) *E. coli* expressing CPO. B: purified CPO after Ni-NTA column (lane 3) and lower molecular weight markers (lane 4).

The SeMet-CPO was expressed in B834 (DE3) cells at a level of 5 mg of pure protein per culture litre. Complete SeMet incorporation was verified by ES-MS. The obtained molecular mass, 35718 Da results from 35390 Da for the recombinant CPO (obtained by ES-MS) plus seven Selenium substituted methionine residues (~328 Da).

6.2.2 Biochemical Characterisation

6.2.2.1 Structural Integrity and Enzymatic Activity

The structural integrity of the purified protein was confirmed by CD spectroscopy. The CD spectrum of purified CPO is typical for a protein containing both α-helices and β-sheets with a broad minimum between 208 and 222 nm as well as an intense positive band at 195 nm (Fig. 22). Evaluation of the spectrum using the program CONTIN (Provencher and Glockner, 1981) resulted in an estimate of 26% α-helices, 31% β-sheets, with the reminder been turns and loops. This estimation is in good agreement with the predicted secondary structure (PredictProtein Tool: http://dodo.cpmc.columbia.edu/predictprotein/). The CD spectrum from the SeMet substituted protein showed a secondary structure content similar to CPO.

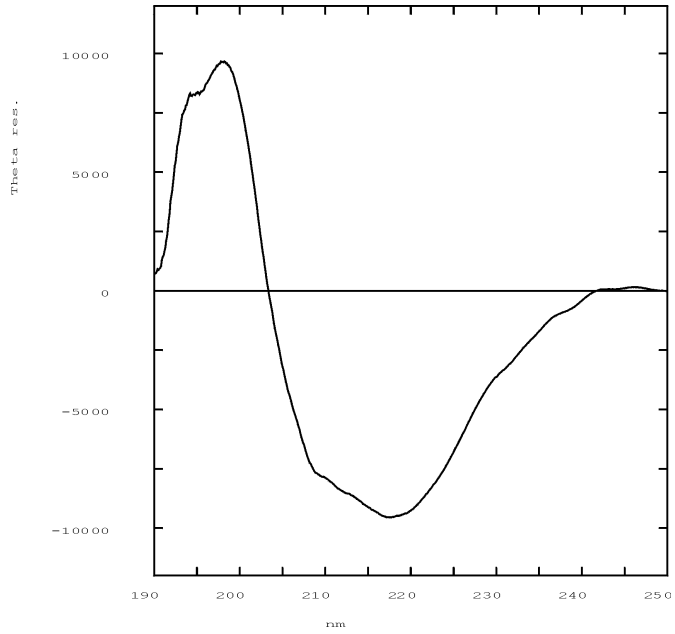

Figure 22 - CD spectrum from *E. coli* CPO (0.15 mg ml^{-1} in 10 mM MES/NaOH pH 6.5) at 20 °C.

The specific activity for both CPO and SeMet-CPO was determined to be approximately 620 nmoles h^{-1} mg^{-1}. This value is lower than those reported for CPO from other sources (Camadro *et al.*, 1986; Kohno *et al.*, 1996; Martasek *et al.*, 1997; Yoshinaga, 1997; Sorianello *et al.*, 2000), indicating a probable mixture population of active and inactive molecules. However, the consummated substrate was not proportional to product formation indicating that first, the substrate may not be catalised by the enzyme, or second, the substrate

is converted into protoporphyrinogen-IX but its slowly oxidation to protoporphyrin-IX (the detectable molecule in the assay) masks the results. To overcome this the enzymatic assays were performed in the presence of a three-fold excess of protoporphyrinogen-IX oxidase (PPO), the enzyme responsible for the oxidation of protoporphyrinogen-IX to protoporphyrin-IX. Whereas the initial specific activity (in the absence of PPO) was roughly of 230 nmol h^{-1} mg^{-1}, the presence of PPO in the assay mixture resulted in a four fold increase, reaching values of approximately 620 nmol h^{-1} mg^{-1}. The presence of copper and iron was assessed by ICP-AES. Iron content was 1.25 mol (Fe) mol^{-1} (protein) for CPO and 0.2 mol (Fe) mol^{-1} (protein) for SeMet-CPO, and copper was barely detectable (around 0.03 (Cu) mol^{-1} (protein) in both samples.

6.2.2.2 Identification of the co-purified Porphyrin

CPO containing fractions presented a faint yellow colour. The UV/Visible spectrum recorded to calculate the protein concentration showed an extra absorption band around 400 nm, typical for porphyrin containing proteins. Upon concentration, the protein solution was light red and 5 absorption bands were now clearly observed (Fig. 23). Fluorescence spectra (excitation at 666nm and emission at 460nm) confirmed the presence of a porphyrin compound.

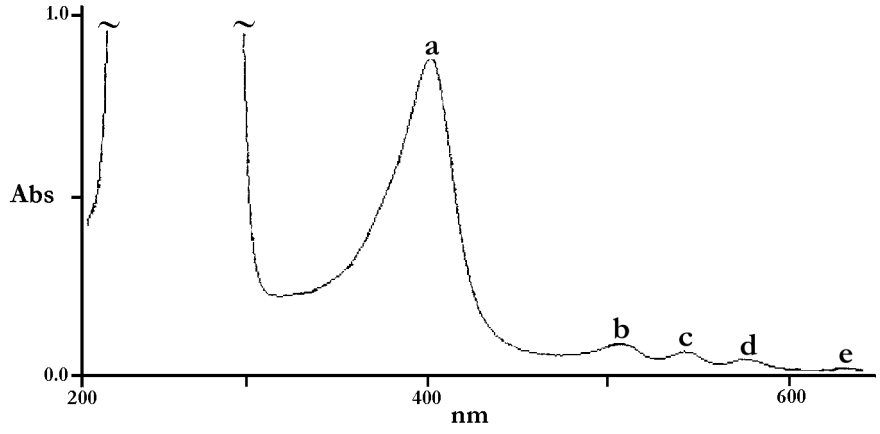

Figure 23 - Absorption spectrum from *E. coli* CPO (5 mg ml^{-1} in 10 mM MES/NaOH pH 6.5).

Letters a to e indicate the absorption peaks typical for a porphyrin compound (~ 400, 500, 540, 580 and 630nm).

To identify this compound, an organic phase extraction was performed and the resulting aqueous and organic phases analysed by ES-MS. Two peaks were obtained at 563.41 Da (minor) and at 581.21 Da (major). The minor one is in good agreement with the molecular weight for the oxidised product, protoporphyrin-IX (562.66 Da). The lability of the vinyl groups from rings B and C makes protoporphyrin-IX an unstable compound, which can easily hydrate to give its isomer derivative deuteroporphyrin IX 2,4 (4,2) hydroxylethyl vinyl. The molecular weight for this isomer, 580.68 Da is in good agreement with the calculated mass for the major peak.

Albeit not stoichiometric, the association of the porphyrin to CPO appears specific since the molecule remained bound even after extensive buffer dialysis. A similar tight interaction was observed between the homologous human protein and the enzyme's substrate, coproporphyrinogen-III (Martasek *et al.*, 1997), (Medlock and Dailey, 1996). Thus suggesting that these interactions may be of physiologic relevance rather then an artefact from the purification.

6.2.2.3 Oligomerisation State in Solution

Size exclusion chromatography in buffers B and E resulted in one single peak corresponding to a molecular weight of approximately 50 kDa (Fig. 24), roughly 1.4 times the mass of the monomer. Whereas the retention time for the protein elution kept similar in higher salt concentrations (buffers C and D), the absence of salt (buffer A) decreased it, indicating a hydrophobic character for the enzyme.

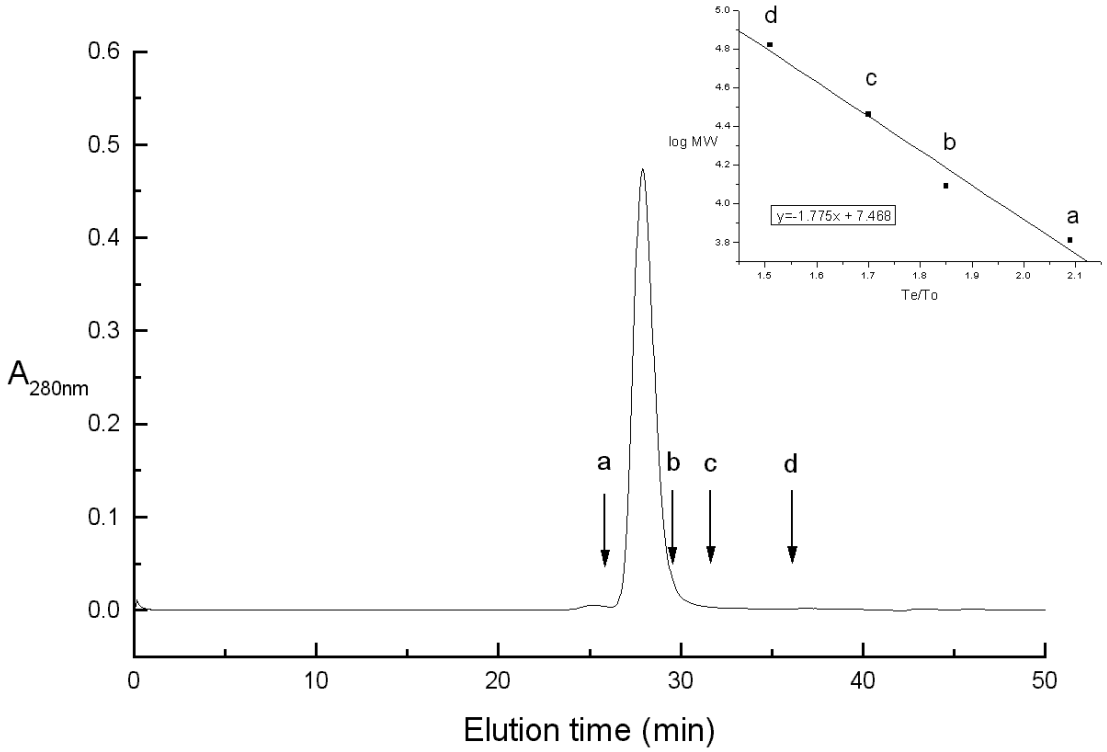

Figure 24 – Size exclusion chromatography from *E. coli* CPO. Purified CPO (5 mg ml^{-1} in 10 mM MES/NaOH pH 6.5) was eluted with buffer E. The vertical arrows indicated the elution times (Te) for calibration proteins, namely BSA (bovin serum albumine), 66 kDa (a), Carbonic anydrase, 29 kDa (b), Cytochrome c, 12.4 kDa (c) and Aprotinin, 6.5 kDa (d). The column's calibration curve is depicted in the right upper corner of the figure. The column's void volume (To) was accessed with Blue Dextran, 2000 kDa.

Similar molecular weight estimations were obtained by DLS. In this method, the molecular weight is calculated assuming a globular conformation model. Considering the protein's molecular size (roughly 35 kDa), these results suggested either an elongated monomer or most probably a globular dimer with a compact shape. Analysis of the protein by gradient native-PAGE (Fig. 25) revealed one band with apparent molecular mass of 70 kDa, consistent with a dimer.

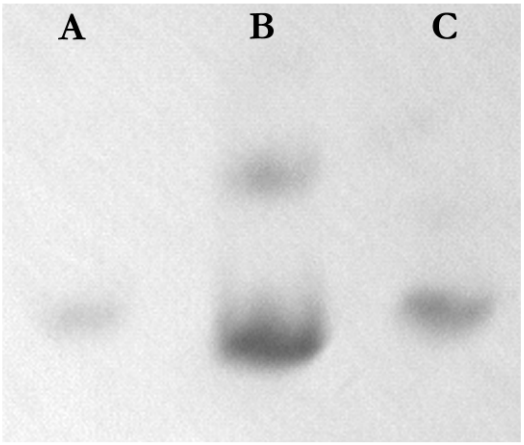

Figure 25 – Gradient (8 to 12.5 %) native-PAGE from *E. coli* CPO. Lanes A and C: CPO at 0.25 mg ml^{-1} and 1 mg ml^{-1}, respectively; lane B: BSA (66 kDa) 2 mg ml^{-1}.

Gel filtration, DLS and native PAGE analysis suggests the protein may be a dimer with a compact shape. This compactness is most probably due to its hydrophobic character. In line with this, homologous proteins from other sources have been reported to have their enzymatic activity stimulated by phospholipids and detergents ((Sorianello and Mazzetti, 2000) and references within). Thus corroborating with the reported association of the protein with membranes.

Biochemical studies have identified several residues essential for enzymatic activity (Yoshinaga and Sano, 1980), (Camadro *et al.*, 1986), (Jones *et al.*, 1997), (Sorianello and Mazzetti, 2000), namely, tyrosine, arginine, lysine, histidine and cysteine. Whereas tyrosine, arginine, lysine and histidine residues seem to be involved either in catalysis or in dimer stabilisation, the involvement of cysteines in any of these features remained controversial. The molecular weight estimations obtained by both gel filtration and DLS were not altered by the presence of DTT (buffers F and G) indicating that disulfide bridges are not involved in the dimer formation and /or stabilisation.

6.2.3 Crystallisation Studies

Initial needle bundles from CPO (5 mg ml^{-1} in 10 mM MES/NaOH pH 6.5) were obtained at 20 °C in 200 mM ammonium acetate, 10 mM magnesium acetate, 50 mM sodium cacodylate pH 6.5, 30% (w/v) PEG 8K. The addition of 5 % xylitol (30 % w/v) improved the crystal's growth and morphology resulting in thin long plates. Next, the composition and

concentration of the reservoir were changed in an attempt to improve the crystal's size and habit. Thicker plates were obtained in the presence of 28 or 30 % PEG 8K, depending on the protein batch. These plates with dimensions roughly of 200 x 100 x 30 μm^3 (Fig. 26) showed a weak but well ordered diffraction power (~ 8 - 6 Å), most probably due to their small size. The crystal plates obtained with SeMet-CPO have similar morphology but with smaller dimensions.

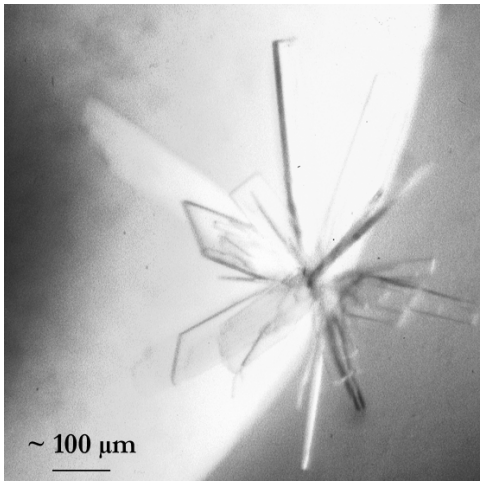

Figure 26 - Crystal plates of *E. coli* CPO grown from 200 mM ammonium acetate, 10 mM magnesium acetate, 50 mM cacodylate pH 6.5, 28 or 30 % PEG 8K, 5 % xylitol at 20 °C.

7 CONCLUSIONS and FUTURE PERSPECTIVES

7.1 Tobacco Uroporphyrinogen-III Decarboxylase

The structural analysis of tobacco UROD (this work) and its comparison with the homologous human enzyme (Whitby *et al*., 1998) conclusively allows the assignment of one sole catalytic cleft per monomer.

Several residues proposed to interact with the substrate are flexible or disordered, resulting most probably from the absence of stabilising interactions with bound substrate. Some of these residues are localised in the loops of the *funnel*, suggesting that the enzyme incorporates other mobile motifs besides the flexible lid region (loop L2) that wrap around the cleft upon substrate insertion.

Once inside the catalytic cleft, uro-III must be shielded from solvent contact for catalysis to take place (Akhtar, 1994). This implies the presence of residues specifically clustered to maximise the insertion of the substrate into this less *attractive* hydrophobic cleft. The *funnel* architecture seems to be structurally optimised to attract the substrate into the catalytic cleft and to protect it from bulk solvent. The importance of this assembly is reflected by its considerable degree of amino acid conservation in all known UROD sequences.

The observed plasticity within the catalytic cleft and flanking regions can explain the remarkable combination of substrate's specificity and promiscuity displayed by UROD (Akhtar, 1994).

Dimer formation brings the unprotected flanks from both catalytic clefts adjacent to one another resulting in a better substrate shielding. Several biochemical and structural studies argue in favour of a dimer-dependent catalysis:

- The absence of natural mutants for residues located at the dimer interface;
- The relatively high degree of amino acid conservation for protein regions buried upon dimerisation;
- The association of activity with a molecular mass corresponding to the dimer (Grimm, B., unpublished results);

• The presence of similar dimers in the crystal structures of tobacco and human UROD;

• The modelling calculations.

A dimer-dependent catalysis can explain why the decarboxylation of the first intermediate is the rate-limiting step in the catalytic reaction (Straka and Kushner, 1983), and the accumulation of its oxidised form in leaves after treatment with Cs^+ (Shalygo *et al.*, 1997). This ion inhibits the uptake of potassium ions from the cytosol into the chloroplast, deregulating the ionic balance within the stroma (Möck, H.-P., unpublished results; for a review in higher plant plastids see (Neuhaus and Wagner, 2000)), which may destabilise the dimer. Whether the dimer is the active unit *in vivo* still needs to be verified by biochemical and structural analysis of protein-protein and protein-ligand complexes.

The present structural and modelling analysis of the two UROD crystal structures answers some intriguing questions concerning the unique catalytic UROD mechanism. For instance:

• The role of Asp82 (localised in a hydrophobic surrounding) in orientating the pyrrole ring moiety to favour the protonation of the α-position by Tyr159;

• The presence of a positively charged side chain, Arg32, which acts as a steering group *helping* the substrate insertion into the hydrophobic catalytic cleft.

Moreover, the analysis of tobacco UROD crystal structure, together with its comparison with the human enzyme, will contribute to delineate future structural based investigations both using substrate analogues and inhibitors, and site-directed mutagenesis.

7.2 *E. coli* Oxygen-dependent Coproporphyrinogen-III Oxidase

Recombinant *E. coli* oxygen-dependent coproporphyrinogen-III oxidase was over-expressed up to 20 mg of pure homogeneous protein per culture litre.

The relative high amounts of protein obtained from the one-step purification permitted the biochemical characterisation and, for the first time initial crystallisation studies for a representative member of the oxygen-dependent CPO family.

A single molecular species was detected by mass spectrometry and its molecular mass is consistent with that of the recombinant his-tagged protein. CD spectroscopy confirmed the structural integrity of the purified protein.

Despite the structural homogeneity of the enzyme preparations, the specific activity is relatively low (620 nmoles h^{-1} mg^{-1}) when compared with homologous proteins (Camadro *et al.*, 1986; Kohno *et al.*, 1996; Martasek *et al.*, 1997; Yoshinaga, 1997; Sorianello *et al.*, 2000). A mixture of active (free enzyme) and product-loaded species in solution could account for this low specific activity. This mixed population may result from the non-stoichiometrically trapping of the product inside the enzyme. Additionally, the different metal content obained for CPO and SeMet-CPO suggests that a metal dependence at least for iron can be ruled out to explain the observed low specific activity. Further studies are necessary to verify the possible interference of the His6-tag on the product's trapping / releasing.

Gel filtration, DLS and native PAGE clearly indicated that CPO is a dimer in solution, and that this dimeric form has a compact shape most probably due to hydrophobic interaction at the protein's surface. This hydrophobic character of the dimer interface corroborates well with the reported association of CPO with membranes. Such an association may facilitate the substrate channelling to the next pathway's enzyme (tightly associated with membranes), and in parallel diminish the risk of loosing the highly photosensitive reaction intermediates.

The similar oligomerisation state reported for all characterised CPOs strongly indicates a putative physiological relevance for the dimer and that it may be a common property of this enzyme family. Moreover, the tight association between human CPO and copro-III, the reaction substrate (Martasek *et al.*, 1997), (Medlock and Dailey, 1996)) and between bacterial CPO and its oxidised product (present work) suggests that the dimer is probably the active unit *in vivo*.

First crystallisation conditions were obtained for CPO resulting in plate-shaped crystals with a week but ordered diffraction quality. The plates reproduced with SeMet-CPO had smaller dimensions. The mixed population with free enzyme and enzyme-product aggregates most probably accounts for the difficulties encountered in growing larger crystals. The presence of product associated with the enzyme is a good starting point for further structural and mechanistic studies.

8 REFERENCES

Akhtar, M. (1994). The modification of acetate and propionate side chains during the biosynthesis of haem and chlorophylls: mechanistic and stereochemical studies. *In The Biosynthesis of Tetrapyrrole Pigments, Ciba Found. Symp.*. Wiley, Chichester, **180**, 131-152.

Akhtar, M., Abboud, M.M., Barnard, G., Jordan, P. and Zaman, Z. (1976). Mechanism and stereochemistry of enzymic reactions involved in porphyrin biosynthesis. *Phil. Trans. R. Soc. London - Series B: Biol. Sci.*, **273**, 117-136.

Al-Karadaghi, S., Hansson, M., Nikonov, S., Jonsson, B. and Hederstedt, L. (1997). Crystal structure of ferrochelatase: the terminal enzyme in heme biosynthesis. *Structure*, **5**, 1501-1510.

Barnard, G.F. and Akhtar, M. (1975). Stereochemistry of Porphyrinogen Carboxy-lyase Reaction in Haem Biosynthesis. *J.C.S. Chem. Comm.*, 494-496.

Barnard, G.F. and Akhtar, M. (1979). Stereochemical and mechanistic studies on the decarboxylation of uroporphyrinogen III in haem biosynthesis. *J. Chem. Soc. Perk. Trans.* 1, **10**, 2354-2360.

Beale, S.I. (1994). Biosynthesis of cyanobacterial tetrapyrrole pigments: Hemes, chlorophyll, and phyvobilins. *In Molecular biology of cyanobacteria*. Bryant, D.A. (ed.). Dordrecht, Kluwer Academic Publishers, pp. 519-580.

Beale, S.I. (1999). Enzymes of chlorophyll biosynthesis. *Photosynth. Res.*, **60**, 43-73.

Beale, S.I. and Castelfranco, P.A. (1973). 14 C incorporation from exogenous compounds into -aminolevulinic acid by greening cucumber cotyledons. *Biochem. & Biophys. Res. Comm.*, **52**, 143-149.

Blundell, T.L. and Johnson, L.N. (1976). *Protein Crystallography*. San Diego, USA, Academic Press Inc..

Brünger, A.T., Adams, P.D., Clore, G.M., Delano, W.L., Gros, P., Grosse Kunstleve, R.W., Jiang, J.S., Kuszewski, J., Nilges, M., Pannu, N.S., Read, R.J., Rice, L.M., Simonson, T. and Warren, G.L. (1998). Crystallography and NMR system: A new software suite for macromolecular structure determination. *Acta Cryst.*, **D54**, 905-921.

Budisa, N., Steipe, B., Demange, P., Eckerskorn, C., Kellermann, J. and Huber, R. (1995). High-level biosynthetic substitution of methionine in proteins by its analogs 2-

aminohexanoic acid, selenomethionine, telluromethionine and ethionine in Escherichia coli. *Eur. J. Biochem.*, **230**, 788-796.

Camadro, J.M., Chambon, H., Jolles, J. and Labbe, P. (1986). Purification and properties of coproporphyrinogen oxidase from the yeast Saccharomyces cerevisiae. *Eur. J. Biochem.*, **156**, 579-587.

Collaborative Computational Project No. 4. (1994). The CCP4 Suite: Programs for protein crystallography. *Acta Cryst.*, **D50**, 760-763.

Conte, L.L., Chothia, C. and Janin, J. (1999). The atomic structure of protein-protein recognition sites. *J. Mol. Biol.*, **285**, 2177-2198.

Crockett, N., Alefounder, P.R., Battersby, A.R., Abell, C. (1991). Uroporphyrinogen III synthase: Studies on its mechanism of action, molecular biology and biochemistry. *Tetrahedron*, **47**, 6003-6014.

Dailey, H.A., Dailey, T.A., Wu, C.K., Medlock, A.E., Wang, K.F., Rose, J.P. and Wang, B.C. (2000). Ferrochelatase at the millennium: structures, mechanisms and [2Fe-2S] clusters. *Cell. & Mol. L. Sci.*, **57**, 1909-1926.

Dailey, H.A., Sellers, V.M. and Dailey, T.A. (1994). Mammalian ferrochelatase. Expression and characterization of normal and two human protoporphyric ferrochelatases. *J. Biol. Chem.*, **269**, 390-395.

Dasgupta, S., Iyer, G.H., Bryant, S.H., Lawrence, C.E. and Bell, J.A. (1997). Extent and nature of contacts between protein molecules in crystal lattices and between subunits of protein oligomers. *Proteins*, **28**, 494-514.

de Verneuil, H., Sassa, S. and Kappas, A. (1983). Purification and properties of uroporphyrinogen decarboxylase from human erythrocytes. A single enzyme catalyzing the four sequential decarboxylations of uroporphyrinogens I and III. *J. Biol. Chem.*, **258**, 2454-60.

Drenth, J. (1994). *Principles of Protein X-Ray Crystallography*. New York, USA, Springer-Verlag.

Elder, G.H. and Roberts, A.G. (1995). Uroporphyrinogen decarboxylase. *J. Bioenerg. & Biomemb.*, **27**, 207-214.

Elder, G.H. and Worwood, M. (1998). Mutations in the hemochromatosis gene, porphyria cutanea tarda, and iron overload. *Hepatology*, **27**, 289-291.

Erskine, P.T., Senior, N., Awan, S., Lambert, R., Lewis, G., Tickle Ian, J., Sarwar, M., Spencer, P., Thomas, P., Warren Martin, J., Shoolingin-Jordan Peter, M., Wood Steve, P. and Cooper Jon, B. (1997). X-ray structure of 5-aminolaevulinate dehydratase, a hybrid aldolase. *Nat. Struct. Biol.*, **4**, 1025-1031.

Esnouf, R.M. (1997). An extensively modified version of MolScript that includes greatly enhanced coloring capabilities. *J. Mol. Graph.*, **15**, 132-143.

Felix, F. and Brouillet, N. (1990). Purification and properties of uroporphyrinogen decarboxylase from Saccharomyces cerevisiae. Yeast uroporphyrinogen decarboxylase. *Eur. J. Biochem.*, **188**, 393-403.

Ferreira, G.C., Franco, R., Lloyd, S.G., Moura, I., Moura, J.J. and Huynh, B.H. (1995). Structure and function of ferrochelatase. *J. Bioenerg. & Biomem.*, **27**, 221-229.

Frankenberg, N., Erskine, P.T., Cooper Jon, B., Shoolingin-Jordan Peter, M., Jahn, D. and Heinz Dirk, W. (1999). High resolution crystal structure of a Mg2+-dependent porphobilinogen synthase. *J. Mol. Biol.*, **289**, 591-602.

Garey, J.R., Labbe-Bois, R., Chelstowska, A., Rytka, J., Harrison, L., Kushner, J. and Labbe, P. (1992). Uroporphyrinogen decarboxylase in Saccharomyces cerevisiae. HEM12 gene sequence and evidence for two conserved glycines essential for enzymatic activity. *Eur. J. Biochem.*, **205**, 1011-1016.

Gibson, K.D., Laver, W.G., Neuberg, A. (1958). Formation of delta-aminolevulinc acid in vitro from succinyl-coenzyme a and glycine. *Biochem J.*, **70**, 71-81.

Gibson, L.C., Marrison, J.L., Leech, R.M., Jensen, P.E., Bassham, D.C., Gibson, M. and Hunter, C.N. (1996). A putative Mg chelatase subunit from Arabidopsis thaliana cv C24. Sequence and transcript analysis of the gene, import of the protein into chloroplasts, and in situ localization of the transcript and protein. *Plant Physiol.*, **111**, 61-71.

Glusker, J.P., Lewis, M. and Rossi, M. (1994). *Crystal Structure Analysis for Chemists and Biologists*. Weinheim, Germany, VCH Verlagsgesellschaft GmbH.

Grafe, S., Saluz, H.P., Grimm, B. and Hanel, F. (1999). Mg-chelatase of tobacco: the role of the subunit CHL D in the chelation step of protoporphyrin IX. *Proc. Natl. Acad. Sci.*, **96**, 1941-1946.

Granik, S. (1950). The structural and functional relationships between heme and chlorophyll. *Harvey Lect*, **44**, 220-245.

Grimm, B. (1998). Novel insights in the control of tetrapyrrole metabolism of higher plants. *Curr. Op. Plant Biol.*, **1**, 245-250.

Guex, N. and Peitsch, M.C. (1996). Swiss-Pdb Viewer: A fast and easy-to-use PDB viewer for Macintosh and PC. *PDB Quart. Newslett.*, **77**, 7-10.

Hennig, M., Grimm, B., Contestabile, R., John, R.A. and Jansonius, J.N. (1997). Crystal structure of glutamate-1-semialdehyde aminomutase: an alpha2-dimeric vitamin B6-

dependent enzyme with asymmetry in structure and active site reactivity. *Proc. Natl. Acad. Sci.*, **94**, 4866-4871.

Heukeshoven, J. and Dernick, R. (1985). Simplified method for silver staining of proteins in polyacrylamide gels and mechanism of silver staining. *Electroforesis*, **6**, 103-108.

Hill, K.L. and Merchant, S. (1995). Coordinate expression of coproporphyrinogen oxidase and cytochrome c6 in the green alga Chlamydomonas reinhardtii in response to changes in copper availability. *EMBO J.*, **14**, 857-865.

Hoober, J.K., Kahn, A., Ash, D.E., Gough, S. and Kannangara, C.G. (1988). Biosynthesis of delta-aminolevulinate in greening barley leaves. IX. Structure of the substrate, mode of gabaculine inhibition, and the catalytic mechanism of glutamate 1-semialdehyde aminotransferase. *Carlsberg Res. Comm.*, **53**, 11-25.

Hu, G., Yalpani, N., Briggs, S.P. and Johal, G.S. (1998). A porphyrin pathway impairment is responsible for the phenotype of a dominant disease lesion mimic mutant of maize [see comments]. *Plant Cell*, **10**, 1095-1105.

Huang, D.D., Wang, W.Y., Gough, S.P. and Kannangara, C.G. (1984). delta-Aminolevulinic acid-synthesizing enzymes need an RNA moiety for activity. *Science*, **225**, 1482-1484.

Hubbard, S.J., Campbell, S.F. and Thornton, J.M. (1991). Molecular Recognition Conformational Analysis of Limited Proteolytic Sites and Serine Proteinase Protein Inhibitors. *J. Mol. Biol.*, **220**, 507-530.

Ishida, T., Yu, L., Akutsu, H., Ozawa, K., Kawanishi, S., Seto, A., Inubushi, T. and Sano, S. (1998). A primitive pathway of porphyrin biosynthesis and enzymology in Desulfovibrio vulgaris. *Proc. Natl. Acad. Sci.*, **95**, 4853-4858.

Jackson, A.H., Ferramola, A.M., Sancovich, H.A., Evans, N., Matlin, S.A., Ryder, D.J. and Smith, S.G. (1976a). Hepta- and hexa-carboxylic porphyrinogen intermediates in haem biosynthesis. *Annals Clin. Research*, **8**, 64-69.

Jackson, A.H., Sancovich, H.A., Ferramola, A.M., Evans, N., Games, D.E., Matlin, S.A., Elder, G.H. and Smith, S.G. (1976b). Macrocyclic intermediates in the biosynthesis of porphyrins. *Phil. Trans. R. Soc. London - Series B: Biol. Sci.*, **273**, 191-206.

Jacobs, J.M. and Jacobs, N.J. (1987). Oxidation of protoporphyrinogen to protoporphyrin, a step in chlorophyll and haem biosynthesis. Purification and partial characterization of the enzyme from barley organelles. *Biochem. J.*, **244**, 219-224.

Jacobs, J.M. and Jacobs, N.J. (1993). Porphyrin accumulation and export by isolated barley (Hordeum vulgare) plastids. Plant Physiol., **101**, 1181-1187.

Jacobs, J.M. and Jacobs, N.J. (1995). Terminal enzymes of heme biosynthesis in the plant plasma membrane. *Arch. Biochem. & Biophys.*, **323**, 274-278.

Jaffe, E.K. (2000). The porphobilinogen synthase family of metalloenzymes. *Acta Cryst.*, **D56**, 115-128.

Jahn, D. (1992). Complex formation between glutamyl-tRNA synthetase and glutamyl-tRNA reductase during the tRNA-dependent synthesis of 5-aminolevulinic acid in Chlamydomonas reinhardtii. *FEBS Letters*, **314**, 77-80.

Janin, J. and Rodier, F. (1995). Protein-protein interaction at crystal contacts. *Proteins*, **23**, 580-587.

Jensen, P.E., Willows, R.D., Petersen, B.L., Vothknecht, U.C., Stummann, B.M., Kannangara, C.G., von Wettstein, D. and Henningsen, K.W. (1996). Structural genes for Mg-chelatase subunits in barley: Xantha-f, -g and -h. *Mol. & Gen. Genet.*, **250**, 383-394.

Jones, M.A., Hamilton, M.L. and Lash, T.D. (1997). Effect of covalent modification on coproporphyrinogen oxidase from chicken red blood cells. *Prep. Biochem. & Biotechnol.*, **27**, 47-57.

Jordan, P.M., Seehra, J.S. (1980). Mechanism of action of 5-aminolevulinic acid dehydratase: Stepwise order of addition of the two molecules of 5-aminolevulinic acid in the enzymic synthesis of porphobilinogen. *J. Chem. Soc. Chem. Commun.*, 240-242.

Kannangara, C.G., Gough, S.P., Bryant, P., Hoober, J.K., Kahn, A., Wettstein, D. (1988). tRNA(Glu) as a cofactor in delta-aminolevulinate biosynthesis: steps that regulate chlorophyll synthesis. *Trends Biochem. Sci.*, **13**, 139-143.

Kannangara, C.G., Vothknecht, U.C., Hansson, M. and von Wettstein, D. (1997). Magnesium chelatase: association with ribosomes and mutant complementation studies identify barley subunit Xantha-G as a functional counterpart of Rhodobacter subunit BchD. *Mol. & Gen. Genet.*, **254**, 85-92.

Kappas, A., Sassa, S., Galbraith, R.A., Nordmann, Y. (1995). *The Porphyrias*. New York, USA, McGraw-Hill.

Kawanishi, S., Seki, Y. and Sano, S. (1983). Uroporphyrinogen decarboxylase. Purification, properties, and inhibition by polychlorinated biphenyl isomers. *J. Biol. Chem.*, **258**, 4285-4292.

Kessel, D. (1984). Porphyrin localization: a new modality for detection and therapy of tumors. B*iochem. Pharmacol*., **33**, 1389-1393.

Kikuchi, G., Kumar, A, Talmage, P., Shemin, D. (1958). The enzymatic synthesis of delta-aminolevulinic acid. *J. Biol. Chem.*, **233**, 1214-1219.

Klemm, D.J., Barton, L.L. (1987). purification and properties of protoporphyrinogen oxidase from an anerobic bacterium, Desulfovibrio gigas. *J. Bacteriol.*, **169**, 5209-5215.

Kohno, H., Furukawa, T., Tokunaga, R., Taketani, S. and Yoshinaga, T. (1996). Mouse coproporphyrinogen oxidase is a copper-containing enzyme: expression in Escherichia coli and site-directed mutagenesis. *Biochim. Biophys. Acta*, **1292**, 156-162.

Kruse, E., Mock, H.P. and Grimm, B. (1995a). Coproporphyrinogen III oxidase from barley and tobacco–sequence analysis and initial expression studies. *Planta*, **196**, 796-803.

Kruse, E., Mock, H.P. and Grimm, B. (1995b). Reduction of coproporphyrinogen oxidase level by antisense RNA synthesis leads to deregulated gene expression of plastid proteins and affects the oxidative defense system. *EMBO J.*, **14**, 3712-3720.

Kruse, E., Mock, H.P. and Grimm, B. (1997). Isolation and characterisation of tobacco (Nicotiana tabacum) cDNA clones encoding proteins involved in magnesium chelation into protoporphyrin IX. *Plant Mol. Biol.*, **35**, 1053-1056.

Labbe, P., Camadro, J.M. and Chambon, H. (1985). Fluorometric assays for coproporphyrinogen oxidase and protoporphyrinogen oxidase. *Analyt. Biochem.*, **149**, 248-260.

Laemmli, U.K. (1970). Cleavage of structural proteins during the assembly of the head of bacteriophage T4. *Nature*, **227**, 680-685.

Lane, T.M., Shah, B.D., Ridgeway, T.M. & Pelletier, S.L. (1992). *Analytical Ultracentrifugation in Biochemistry and Polymer Science*. Harding, S.E., Rowe, A.J. & Horton, J.C., eds. (Royal Society of Chemistry, Cambridge), pp. 90-125.

Lash, T.D. (1991). Action of uroporphyrinogen decarboxylase on uroporphyrinogen-III: a reassessment of the clockwise decarboxylation hypothesis. *Biochem. J.*, **278**, 901-903.

Lash, T.D., Hall, T., Mani, U.N., Jones, M.A. (2001). Normal and abnormal heme biosynthesis. 3.(1) synthesis and metabolism of tripropionate analogues of coproporphyrinogen-iii: novel probes for the active site of coproporphyrinogen oxidase. *J. Org. Chem.*, **66**, 3753-3759.

Laskowski, R., MacArthur, M., Hutchinson, E. and Thorton, J. (1993). PROCHECK: a program to check the stereochemical quality of protein structures. *J. Appl. Cryst.*, **26**, 283-291.

Lehmann, C., Schweizer, B., Leumann, C. and Eschenmoser, A. (1997). Chemistry of Alpha-Aminonitriles - Regioselective Synthesis and Crystal Structure of Uroporphyrinogen (Type I) Octanitrile. *Helv. Chim. Acta*, **80**, 1421-1442.

Lehnen, L.P., Jr., Sherman, T.D., Becerril, J.M. and Duke, S.O. (1990). Tissue and Cellular Localization of Acifluorfen-Induced Porphyrins in Cucumber Cotyledons. *Pest. Biochem. & Physiol.*, **37**, 239-248.

Lermontova, I., Kruse, E., Mock, H.P. and Grimm, B. (1997). Cloning and characterization of a plastidal and a mitochondrial isoform of tobacco protoporphyrinogen IX oxidase. *Proc. Natl. Acad. Sci.*, **94**, 8895-900.

Loeb, M.R. (1995). Ferrochelatase activity and protoporphyrin IX utilization in *Haemophilus influenzae*. *J. Bacteriol.*, **177**, 3613-3615.

Louie, G.V., Brownlie, P.D., Lambert, R., Cooper, J.B., Blundell, T.L., Wood, S.P., Warren, M.J., Woodcock, S.C. and Jordan, P.M. (1992). Structure of porphobilinogen deaminase reveals a flexible multidomain polymerase with a single catalytic site. *Nature*, **359**, 33-39.

Luo, J. and Lim, C.K. (1993). Order of uroporphyrinogen III decarboxylation on incubation of porphobilinogen and uroporphyrinogen III with erythrocyte uroporphyrinogen decarboxylase. *Biochem. J.*, **289**, 529-532.

Martasek, P., Camadro, J.M., Raman, C.S., Lecomte, M.C., Le Caer, J.P., Demeler, B., Grandchamp, B. and Labbe, P. (1997). Human coproporphyrinogen oxidase. Biochemical characterization of recombinant normal and R231W mutated enzymes expressed in E. coli as soluble, catalytically active homodimers. *Cell. & Mol. Biol.*, **43**, 47-58.

Matthews, B.W. (1968). Solvent content of protein crystals. *J. Mol. Biol.*, **33**, 491-497.

Mauzerall, D.C. (1998). Evolution of Porphyrins. *Clin. Dermatol.*, **16**, 195-201.

McRee, D.E. (1993). *Practical Protein Crystallography*. New York, USA, Academic Press.

Medlock, A.E. and Dailey, H.A. (1996). Human coproporphyrinogen oxidase is not a metalloprotein. *J. Biol. Chem.*, **271**, 32507-32510.

Meller, E., Belkin, S., Harel, E. (1975). The biosynthesis of delta-aminolevulinic acid in greeing maize leaves. *Phytochemistry*, **14**, 2399-2402.

Macromolecular Crystallography (1997). Carter, C.W.Jr., Sweet, R.M. (Ed). *Meth. Enzymol.*, **276**, Part A, Academic Press.

Merrit, E.A. and Bacon, D.J. (1997). Raster3D: Photorealistic Molecular Graphics. *Meth. Enzymol.*, **277**, 505-524.

Mock, H.P., Trainotti, L., Kruse, E. and Grimm, B. (1995). Isolation, sequencing and expression of cDNA sequences encoding uroporphyrinogen decarboxylase from tobacco and barley. *Plant Mol. Biol.*, **28**, 245-256.

Mock, H.-P. and Grimm., B. (1997). Reduction of Uroporphyrinogen Decarboxylase by antisense RNA Expression Affects Activities of Other Enzymes Involved in Tetrapyrrole Biosynthesis and Leads to Light-Dependent Necrosis. *Plant Physiol.*, **113**, 1101-1112.

Nagano, N., Hutchinson, E.G. and Thornton J.M. (1999). Barrel structures in proteins: Automatic identification and classification including a sequence analysis of TIM barrels. *Protein Sci.*, **8**, 2072-2094.

Navaza, J. (1994). An automated package for molecular replacement. *Acta Cryst.*, **A50**, 157-163.

Neuhaus, H.E. and Wagner, R. (2000). Solute pores, ion channels, and metabolite transporters in the outer and inner envelope membranes of higher plant plastids. *Biochim. Biophys. Acta*, **1465**, 307-323.

Nicholls, A., Bharadwaj, R. and Honig, B. (1993). GRASP - graphical representation and analysis of surface properties. *Biophys. J.*, **64**, A166.

Nureki, O., Vassylyev, D.G., Katayanagi, K., Shimizu, T., Sekine, S., Kigawa, T., Miyazawa, T., Yokoyama, S. and Morikawa, K. (1995). Architectures of class-defining and specific domains of glutamyl-tRNA synthetase. *Science*, **267**, 1958-1965.

Otwinowski, Z. and Minor, W. (1996). Processing of X-ray diffraction data collected in oscillation mode. *Meth. Enzymol.*, **276**, 307-326.

Petersen, B.L., Kannangara, C.G. and Henningsen, K.W. (1999). Distribution of ATPase and ATP-to-ADP phosphate exchange activities in magnesium chelatase subunits of Chlorobium vibrioforme and Synechocystis PCC6803. *Arch. Microbiol.*, **171**, 146-150.

Poulson, R. and Polglase, W.J. (1974). Site of glucose repression of heme biosynthesis. *FEBS Letters*, **40**, 258-260.

Provencher, S.W. and Glockner, J. (1981). Estimation of globular protein secondary structure from circular dichroism. *Biochemistry*, **20**, 33-37.

Rose, S., Frydman, R.B., de los Santos, C., Sburlati, A., Valasinas, A. and Frydman, B. (1988). Spectroscopic evidence for a porphobilinogen deaminase-tetrapyrrole complex that is an intermediate in the biosynthesis of uroporphyrinogen III. *Biochemistry*, **27**, 4871-4879.

Sambrook, J., Fritsch, E.F. and Maniatis, T. (1989). *Molecular cloning: A laboratorial manual*. New York, USA, Cold Spring Harbor Laboratory Press.

Sassa, S. and Kappas, A. (2000). Molecular aspects of the inherited porphyrias. *J. Intern. Med.*, **247**, 169-78.

Seehra, J.S., Jordan, P.M. and Akhtar, M. (1983). Anaerobic and aerobic coproporphyrinogen III oxidases of Rhodopseudomonas spheroides. Mechanism and stereochemistry of vinyl group formation. *Biochem. J.*, **209**, 709-718.

Shalygo, N.V., Averina, N.G., Mock, H.P. and Grimm, B. (1997). Influence of cesium on tetrapyrrole biosynthesis in etiolated and greening barley leaves. *Physiol. Plant.,* **99**, 160-168.

Shemin, D., Russell, C.S. (1953). 5-aminolevulinic acid: its role in the biosynthesis of porphyrins and purines. *J Am Chem Soc*, **75**, 4873-4875.

Shoolingin-Jordan, P.M., Warren, M.J. and Awan, S.J. (1996). Discovery that the assembly of the dipyrromethane cofactor of porphobilinogen deaminase holoenzyme proceeds initially by the reaction of preuroporphyrinogen with the apoenzyme. *Biochem. J.*, **316**, 373-376.

Sorianello, E.M. and Mazzetti, M.B. (2000). Function and structure of rat hepatic coproporphyrinogen oxidase. *Comp. Biochem. & Physiol. Part B, Biochem. & Mol. Biol.*, **127**, 155-164.

Straka, J.G. and Kushner, J.P. (1983). Purification and characterization of bovine hepatic uroporphyrinogen decarboxylase. *Biochemistry*, **22**, 4664-4672.

Tait, G.H. (1972). Coproporphyrinogenase activities in extracts of Rhodopseudomonas spheroides and Chromatium strain D. *Biochem. J.*, **128**, 1159-1169.

Troup, B., Hungerer, C. and Jahn, D. (1995). Cloning and characterization of the Escherichia coli hemN gene encoding the oxygen-independent coproporphyrinogen III oxidase. *J. Bacteriol.*, **177**, 3326-3331.

Turk, D. (1992). Weiterentwicklung eines Programms fur Molekulgraphik und Elecktronendichte-Manipulation und seine Anwendung auf verschiedene Protein-Strukturaufklarungen. Technische Universität, München, Germany.

Walker, C.J. and Willows, R.D. (1997). Mechanism and regulation of Mg-chelatase. *Biochem. J.*, **327**, 321-333.

Whitby, F.G., Phillips, J.D., Kushner, J.P. and Hill, C.P. (1998). Crystal structure of human uroporphyrinogen decarboxylase. *EMBO J.*, **17**, 2463-2471.

Willows, R.D., Hansson, M., Beale, S.I., Laurberg, M. and Al-Karadaghi, S. (1999). Crystallization and preliminary X-ray analysis of the Rhodobacter capsulatus magnesium chelatase BchI subunit. *Acta Cryst.*, **D55**, 689-690.

Woods, J.S. (1974). Studies on the role of heme in the regulation of delta-aminolevulinic acid synthetase during fetal hepatic development. *Mol. Pharmacol.*, **10**, 389-397.

Wu, C.K., Dailey, H.A., Rose, J.P., Burden, A., Sellers, V.M. and Wang, B.C. (2001). The 2.0 A structure of human ferrochelatase, the terminal enzyme of heme biosynthesis. *Nat. Struct. Biol.*, **8**, 156-160.

Wyckoff, E.E., Kushner, J.P. (1994). *The Liver: Biology and Pathobiology*. New York, USA, Raven Press Ltd.

Wyckoff, E.E., Phillips, J.D., Sowa, A.M., Franklin, M.R. and Kushner, J.P. (1996). Mutational analysis of human uroporphyrinogen decarboxylase. *Biochim. Biophys. Acta*, **1298**, 294-304.

Yoshinaga, T., Sano, S. (1980). Coproporphyrinogen oxidase. II Reaction mechanism and role of tyrosine residues on the activity. *J. Biol. Chem*, **255**, 4727-4731.

Yoshinaga, T. (1997). Purification and Properties of Coproporphyrinogen III from Bovine Liver. *Meth. Enzymol*., **281**, 355-367.

9 Appendix

9.1 Abbreviations

Å	Ångstrøm; 1 Å = 10^{-10} m
ASA	Accessible surface area
BSA	Bovine Serum Albumin
CD	Circular Dichroism spectroscopy
CPO	Oxygen-dependent Coproporphyrinogen-III oxidase
Copro-III	Coproporphyrinogen-III
Da, kDa	Dalton, kilo Dalton; 1 Da = 1 $gmol^{-1}$
DLS	Dynamic light scattering
DTT	Dithiothreitol
E. coli	*Escherichia coli*
EDTA	Ethylene diamine tetraacetic cid
ES-MS	Electron spray mass spectrometry
HEPES	N-2-hydroxyethylpiperazine-N'-2-ethanesulfonic acid
ICP-AES	Induced-coupled mass-atomic emission spectroscopy
IPTG	Isopropylthiogalactoside
LB	Luria-Bertani (medium)
M	Molar (mol l^{-1})
MES	2-morpholinoethanesulfonic acid
min	minutes
MOPS	3-morpholino-propane sulphonic acid
NM	New Minimal (medium)
OD	Optical Density
SDS-PAGE	Sodium dodecyl sulphate Polyacrylamide gel electrophoresis
PBS	Phosphate buffered saline
PEG	Polyethylenoglycol
Proto-IX	Protoporphyrinogen-IX
r.m.s.d.	root-mean-square deviation

rpm	rotation per minute
RT	Room temperature
SeMet	Seleno-methionine
SeMet-CPO	Selenomethionine substituted CPO
Tobacco	*Nicotiana tabacum*
Tris	N-tris-(hydroxymethyl)- aminomethane
UROD	Uroporphyrinogen-III decarboxylase
v/v	volume per volume
w/v	weight per volume

Amino acids

A	Ala	Alanine	M	Met	methionine
C	Cys	Cysteine	N	Asn	asparagine
D	Asp	Aspartate	P	Pro	proline
E	Glu	Glutamate	Q	Gln	glutamine
F	Phe	Phenylalanine	R	Arg	arginine
G	Gly	Glycine	S	Ser	serine
H	His	Histidine	T	Thr	threonine
I	Ile	Isoleucine	V	Val	valine
K	Lys	Lysine	W	Trp	tryptophan
L	Leu	Leucine	Y	Tyr	tyrosine

9.2 Index of Figures

9.3 Index of Tables

9.4 *Curriculum vitae*

Personal Data

Name	Berta Maria Dias Pereira Martins
Date and Place of Birth	06.01.1971 in Figueira da Foz, Portugal

Education and Research Activities

1989 - 1995 Degree in Applied Chemistry with specialisation in Biotechnology at the New University of Lisbon, Portugal.

1993 - 1994 Internship at the Metalloproteins & Bioenergetics Group headed by Prof. Miguel Teixeira, Institute of Technology for Chemistry and Biology (ITQB), Oeiras, Portugal. Participation in the biochemical studies of an iron-sulphur cluster containing ferredoxin from the thermoacidophilic archaeon *Desulfurolobus ambivalens*.

1994 - 1995 Diploma Thesis at the Molecular Genetics Laboratory headed by Prof. Dr. Claudina Rodrigues-Pousada, Institute Gulbenkian of Science, Oeiras, Portugal. The work's title was "Molecular cloning and sequence analysis of a fragment from the poliscistronic unit of DNA containing the molybdenum aldehyde oxido-reductase (MOPP) from *Desulfovibrio gigas*".

1996 - Present Department of Structural Research headed by Prof. Dr. Robert Huber, FRS, Max-Planck-Institute for Biochemistry, Martinsried, Germany.

1996 – 1998 Fellowship from the Max Planck Society. Determination of the crystal structure from the seven-iron ferredoxin from the thermophilic bacterium *Thermus thermophilus*.

1997 – 2001 Fellowship from the Ph.D. program PRAXIS XXI, Foundation for Science and Technology, Ministry of Science, Portugal. Ph.D. Thesis

with the title "Biochemical and Structural Studies of two Enzymes from the Tetrapyrrole Biosynthetic Pathway: Uroporphyrinogen-III Decarboxylase and Oxygen-dependent Coproporphyrinogen-III Oxidase".

2000 – Present Determination of the crystal structure from the NAD^+-dependent (R)-2-Hydroxyglutarate Dehydrogenase from *Acidaminococcus fermentans*, and the 4-Hydroxybutyryl-CoA Dehydratase from *Clostridium aminobutyricum*.

Courses and Workshops attended

Biotechnology of Extremophiles: First meeting of the pH cluster. ITQB, Oeiras, Portugal. January 15-16, 1994.

X Biotechnology Youth Meeting. Centre for Experimental Cytology, University of Oporto, Portugal. May 12-15, 1994.

Worshop in DNA Technology, Industrial and Technical Engeneering National Institute (INETI), Lisbon, Portugal. Januray 04 - February 10, 1995.

European Science Foundation (ESF) Workshop on *Molecular Recognition in Metalloproteins*. Seville, Spain. October 23-26, 1997.

European Union-ESF Advance Course on Chemistry of *Metals in Biological Systems*. University of Louvain-la-Neuve, Belgium. May 13-22, 1998.

Training and Mobility of Researchers (TMR) Summer School on *Structural and Function of Metalloproteins*. ITQB, Oeiras, Portugal. September 7-19, 1998.

Deutsche Forschungsgemeinchaft (DFG) Priority Program *Radicals in enzymatic catalysis*. Schloß Rauischholzhausen, Philipps-University, Marburg, Germany, April 12-14, 2000.

Deutsche Forschungsgemeinchaft (DFG) Priority Program *Radicals in enzymatic catalysis*. Schloß Rauischholzhausen, Philipps-University, Marburg, Germany, February 12-13, 2001.

Conference Presentations

Martins, B., Flores, O., Neves, A. and Rodrigues-Pousada, C.. The operon for the molybdenum containing aldehyde oxido-reductase of *Desulfovibrio gigas*: molecular cloning and sequence analysis of the DNA policistronic unit. *XXX Luso-Spanish Genetics Meeting*. Lisbon, Portugal, September 21-23, 1995 (Oral communication).

Martins, B.M., Macedo-Ribeiro, S., Pereira, P.J.B., Buse, G., Huber, R. and Soulimane, T.. *Thermus thermophilus* 7Fe Ferredoxin at 1.64 Å resolution: Insights into Bacterial Ferredoxins Thermostability. *9th International Conference on Biological Inorganic Chemistry* (ICBIC'99). Minneapolis, Minnesota, USA, July 11-16, 1999 (Poster communication).

Martins, B.M., Macedo-Ribeiro, S., Çinkaya, I., Buckel, W. and Messerschmidt, A.. Crystallisation of 4-hydroxybutyryl-CoA dehydratase from *Clostridium aminobutyricum*. Deutsche Forschungsgemeinchaft (DFG) Priority Program *Radicals in enzymatic catalysis*. Schloß Rauischholzhausen, Philipps-University, Marburg, Germany, April 12-14, 2000 (Oral communication).

Martins, B.M., Grimm, B., Jacob, U., Huber, R. and Messerschmidt, A.. Uroporphyrinogen-III Decarboxylase from *Nicotiana tabacum*: Dimer-dependent decarboxylation?. Gordon Research Conference (GRC) on *Tetrapyrroles, Chemistry & Biology of*. Newport, Rhode Island, USA, July 16-21 2000. And *MILLENIUM MEETING on PORPHYRINS and PORPHYRIAS 2000*. Institute Pasteur, Paris, France, September 10-13 2000 (Poster communications).

Martins, B.M., Grimm, B., Mock, H.-P., Huber, R. and Messerschmidt, A.. Uroporphyrinogen-III Decarboxylase from *Nicotiana tabacum*: Revisiting its unique Multi-step Decarboxylation. *27th Meeting of the Federation of European Biochemical Societies* (FEBS LISBON'2001), Lisbon, Portugal, June 30 - July 5, 2001. And *International Conference on Bioinorganic Chemistry* (ICBIC'10), Florence, Italy, August 26-31, 2001 (Poster communications).

Publications

Martins, B. M. (1995). Clonagem e sequenciação de um framento de DNA da unidade policistrónica contendo a região codificante para a aldeído oxido-redutase de molibdénio de *Desulfovibrio gigas*. Diploma Thesis, New University of Lisbon, Portugal.

Flores, O., Martins, B., Neves, A. and Pousada, C. (1997). Characterization of the polycistronic unit containing the molybdenum aldehyde oxido-reductase (MOP) of *Desulfovibrio gigas*. *FASEB J*. **11** (9), Suppl S Jul 31, 2074, A1212.

Martins, B.M., Macedo-Ribeiro, S., Pereira, P.J.B., Buse, G., Huber, R. and Soulimane, T. (1999). Thermostability of bacterial ferredoxins: crystal structure of the ferredoxin from *Thermus thermophilus* at 1.64 Å resolution. *J Inorg. Biochem.* **74** (1-4) Apr 30, 222.

Martins, B.M., Macedo-Ribeiro, S., Pereira, P.J.B., Buse, G., Huber, R. and Soulimane, T. (2001). New insights into the thermostability of bacterial ferredoxins: high-resolution crystal structure of the seven-iron ferredoxin from *Thermus thermophilus*. *J Biol. Inorg. Chem.* **6**, 663-674.

Martins, B.M., Grimm, B., Mock, H.-P., Huber, R. and Messerschmidt, A. (2001). Crystal structure and substrate modeling of the uroporphyrinogen-III decarboxylase from *Nicotiana tabacum*: dimer-dependent catalysis. *Eur. J. Biochem*., **268**, Suppl 1 Jul 2001, 171, PS7-029.

Martins, B.M., Grimm, B., Mock, H.-P., Huber, R. and Messerschmidt, A. (2001). Crystal structure and substrate modeling of the uroporphyrinogen-III decarboxylase from *Nicotiana tabacum*: Revisiting its unique Multi-step Decarboxylation. *J Inorg. Biochem.* **86** (1) Aug 2001,329.

Martins, B.M., Grimm, B., Mock, H.-P., Richter, G., Huber, R. and Messerschmidt, A. (2001). Tobacco uroporphyrinogen-III decarboxylase: characterisation, crystallisation and preliminary X-ray analysis. *Acta Crystallogr. Sec. D*. **D57**, 1709-1711.

Martins, B.M., Grimm, B., Mock, H.-P., Huber, R. and Messerschmidt, A. (2001). Crystal structure and substrate modeling of the uroporphyrinogen-III decarboxylase from *Nicotiana tabacum*: Implications for the catalytic mechanism.. *J. Biol. Chem*. **276** (47) Nov 23, 44108-44116.

Martins, B.M., Macieira, S. and Huber, R. (2001). Oxygen-dependent coproporphyrinogen-III oxidase from *Escherichia coli*: one-step purification, biochemical and crystallization studies. ***Submitted for publication***.